

Dalton Transactions

Accepted Manuscript



This is an *Accepted Manuscript*, which has been through the Royal Society of Chemistry peer review process and has been accepted for publication.

Accepted Manuscripts are published online shortly after acceptance, before technical editing, formatting and proof reading. Using this free service, authors can make their results available to the community, in citable form, before we publish the edited article. We will replace this *Accepted Manuscript* with the edited and formatted *Advance Article* as soon as it is available.

You can find more information about *Accepted Manuscripts* in the [Information for Authors](#).

Please note that technical editing may introduce minor changes to the text and/or graphics, which may alter content. The journal's standard [Terms & Conditions](#) and the [Ethical guidelines](#) still apply. In no event shall the Royal Society of Chemistry be held responsible for any errors or omissions in this *Accepted Manuscript* or any consequences arising from the use of any information it contains.

Chiral modification of copper exchanged zeolite-Y with cinchonidine and its application in asymmetric Henry reaction

Jogesh Deka,^a L. Satyanarayana,^b G. V. Karunakar,^c Pradip Kr. Bhattacharyya,^d Kusum K. Bania^{a*}

^aDepartment of Chemical Tezpur University, Assam, India, 784028

^bCenter for NMR and Structural Chemistry, Indian Institute of Chemical Technology, Uppal Road, Tarnaka, Hyderabad, Telangana 500007

^cDivision of Crop Protection Chemicals, Indian Institute of Chemical Technology, Uppal Road, Tarnaka, Hyderabad, Telangana 500007

^dArya Vidyapeeth College, Guwahati, Assam 781016, India.^d

Abstract: Chirally modified Cu²⁺ exchanged zeolite-Y were synthesized by direct adsorption of cinchonidine at ambient condition. The chirally modified materials were characterized using various spectrochemical and physicochemical techniques *viz* BET, FTIR, MAS (¹H, ¹³C NMR), XPS, SEM, Cyclic Voltammetry and PXRD. Characteristics peaks of cinchonidine observed in supported materials confirmed the adsorption of cinchonidine and its co-ordination with Cu²⁺-active site on the copper exchanged zeolite-Y. ¹³C SSNMR and XPS analysis however confirms for the *half encapsulation* process, only the quinoline ring of cinchonidine get coordinated to the internal metal sites *via* N-atom while the quinuclidine moiety extends out of the host surface. Cinchonidine supported Cu²⁺-Y zeolites were found to exhibit good catalytic performance in asymmetric Henry reaction. ¹H-SSNMR studies also confirmed for the protonation of the N-atom of the quinuclidine ring during the course of the Henry reaction. Heterogeneous chiral catalysts were effective upto two consecutive cycles. Leaching of cinchonidine after second cycle was found to have negative results in the catalytic performance.

Key words: Cinchonidine, copper exchanged zeolite-Y, encapsulation, asymmetric Henry reaction

Introduction

Cinchonidine a chiral alkaloid found in the bark of cinchona tree appears to be excellent chiral modifier for solid supports since the report of Orito et al. in late 1970's.¹ Pt/Al₂O₃ modified with cinchonidine supported catalyst found to be efficient catalyst in hydrogenation reaction.²⁻⁷ Such chirally modified Pt based catalysts are found to offers strong stereoselective control along with high activity in the hydrogenation of activated ketones and trifluoroacetophenones.⁸⁻¹⁰ High enantioselectivity on Pt/Al₂O₃ surface is simply achieved by addition of small amount of chiral modifier.¹⁰ Cinchonidine can bind to the metal surface in different nature or can have different conformation during the time of adsorption on solid support.¹¹ In coordination metal complex it may co-ordinate to the metal center by direct-coordination of N-atom of the quinoline ring or it may co-ordinate by the hydroxyl oxygen atom and N-atom of the quinuclidine ring.¹² Xu et al. reported that when cinchonidine adsorbed Cu(111) surface, quinoline rings lies parallel to Cu(111) while the chiral quinuclidine moiety extends out of the substrate surface.¹³ Depending on the nature of binding mode or the adsorption on the surface, property of cinchonidine may change. Further, N-atom of the quinuclidine has the ability to get protonated and the protonated cinchonidine found to have different chemistry from the unprotonated one.¹⁰ Olsen et al. reported that the free rotations around the central C-C bonds were severely impaired on protonation.¹⁴

Zeolite-Y with its pore dimension of 7.4Å and supercage of 13Å found to be excellent host for supramolecular host-guest chemistry.¹⁵⁻¹⁸ With respect to the size of adsorb organic molecule or ligands it can occupy different site of the zeolite cavity. Because of their ability to trap molecule or in other sense molecules of only specific size can diffuse through the channels of zeolite-Y, they have found wide applications in catalysis and petrochemical industries.¹⁹⁻²² Besides zeolite-Y can act as host for encapsulation of various transition metal complexes so called “*Ship in a Bottle*” complexes.²³ Following the pioneering work of Herron various metal complexes has been encapsulated inside the supercage of zeolite-Y.^{24,25} Such kind of encapsulated complexes also reported to have good catalytic activity and in many cases they are found to be superior catalyst then its homogeneous frills.²³ Recent progress in heterogenisation of homogeneous catalyst also reports for the entrapment of chiral catalyst inside the cavity of zeolite-Y.^{16-18,23} Cinchonidine a chiral molecule having different binding mode for transition metals however has not been supported in zeolite-Y. Böhmer et al²⁶ used cinchonidine as chiral

agent in enantioselective hydrogenation of ethyl pyruvate with Pt/zeolite-Y catalyst. But detailed investigation on the interaction of cinchonidine with metal exchanged zeolite-Y is not available in the literature. Possibly the larger dimension of the molecule having quinuclidine ring attached to the quinolone ring *via* C-C bond and steric crowding associated with the quinuclidine ring will probably hinders the encapsulation process. However, there is a possibility that half of the molecule penetrates inside the cavity and a part remains outside the cavity or may be regarded as *half encapsulation* process.²⁷ In the present work we have tried to illustrate the possibility of interaction of cinchonidine with Cu²⁺ exchanged zeolite-Y.

Preparation of Cu²⁺-exchanged zeolite-Y, Cu²⁺-Y

The preparation was done following a reported procedure.²³ NaY-zeolite was heated in air with a rate of 1K min⁻¹ and calcined further at 773 K for 24 hours to burn off organic impurities. Cu²⁺ exchanged zeolite-Y was prepared by stirring 1g of pretreated Na-Y with 50 mL of (0.01)M aqueous CuCl₂.2H₂O solution in a round bottom flask for 48 hours at 298 K. While preparing the samples, the pH of the solutions was maintained within 3-5 using buffer tablets in order to prevent the precipitation of metal hydroxide. Once the stirring was completed, the samples were filtered using Whatman no. 1 filter paper and were washed thoroughly with warm deionized water. The washing was continued until the samples become free from dissolved chloride ion (Cl⁻). Chloride test was performed with the filtrate to confirm the complete removal of chloride ions. The Cu²⁺-exchanged zeolite (Cu²⁺-Y) was then dried well in a hot air oven at 373 K for 12 hours.

Immobilization of cinchonidine with metal-exchanged zeolite-Y, Cu²⁺-Y-CD

(-)-cinchonidine (1mmol, CD) was prepared by dissolving it in acetonitrile. To this solution, 0.5 g of metal-exchanged zeolite-Y was added. The whole reaction mixture was then continuously stirred at 80 °C for 60 h under refluxing conditions.

General procedure for asymmetric nitro-aldol reaction

To a well stirred solution of Cu²⁺-Y-CD (0.15g of catalyst in 5 ml of acetonitrile), aldehyde (5 mmol) was added and allowed the mixture to be stirred further for 15-20 min. The resulting solution was brought to -4 °C and nitromethane (5 mmol) was slowly added in an interval of 1h by using a syringe. The progress of the reaction was checked on TLC. After 48h the product was separated using repetitive washing of the reaction mixture (five times) with hexane ethyl acetate 7:2 mixture. After complete washing, the copper complex was dried under vacuum and

stored in desiccator for its use in subsequent catalytic runs. The enantiomeric excess (ee) of the product was determined by HPLC (High Performance Liquid Chromatography) analysis using chiral columns (ϕ 4.6 mm x 250 mm, DAICEL CHIRALCEL OD-H or CHIRALPAK AD-H).

Materials and characterization

NaY-zeolite, aldehydes, nitromethane and cinchonidine were purchased from Sigma-Aldrich. $\text{CuCl}_2 \cdot 2\text{H}_2\text{O}$ was brought from Merck and all solvent used in this study were HPLC grade from Rankem. Powder X-ray diffraction (PXRD) patterns were recorded on a Shimadzu XD-D1 powder X-ray diffractometer using Cu $K\alpha$ radiation ($\lambda = 1.542 \text{ \AA}$). PXRD patterns were recorded in the 2θ range of $10\text{-}50^\circ$ at a scanning rate of $2^\circ/\text{min}$. Electronic absorption spectra (UV-Vis) were measured using a Hitachi U-3400 spectrophotometer with a diffuse reflectance apparatus equipped with an integrating sphere of 60 mm inner diameter. Mono-chromatic light was used in the whole spectral region in order to minimize the effect of fluorescence. For recording the spectra of the $\text{Cu}^{2+}\text{-Y}$ and $\text{Cu}^{2+}\text{-Y-CD}$, the powdered samples were placed in a black absorbing hole (10 mm, in diameter and 3 mm deep) of a sample holder, and the surface is smoothed. The layer can be regarded as infinitely thick, as required by the Kubelka-Munk theory. The optical spectrums were then recorded in the reflectance mode. A Kubelka-Munk (KM) analysis¹⁷ was performed on the reflectance data. The KM factor, $F(R)$, is given by $F(R) = (1-R)^2/2R = k/s$ where R is the diffuse reflectance of the sample as compared to BaSO_4 , k is the molar absorption coefficient, and s is the scattering coefficient of the sample. Infra-red spectra (FTIR) in the range of $500\text{-}4000 \text{ cm}^{-1}$ were recorded on a Perkin-Elmer Spectrum 2000 FTIR spectrometer. FTIR spectra of $\text{Cu}^{2+}\text{-Y}$ and $\text{Cu}^{2+}\text{-Y-CD}$ were recorded against a zeolite background, which is recorded at 100°C after 1 h of evacuation. The cyclic voltammograms of $\text{Cu}^{2+}\text{-Y}$ and $\text{Cu}^{2+}\text{-Y-CD}$ were recorded using CHI-600A meter from CH Instruments, and 0.1 M TBAP (tetra-butyl ammonium phosphate) was used as the supporting electrolyte. For recording the cyclic voltammogram $\text{Cu}^{2+}\text{-Y}$ and $\text{Cu}^{2+}\text{-Y-CD}$, the working electrode was prepared by taking a 1:1 weight ratio of metal complexes in 1 ml of dichloromethane (DCM). This suspension was ultrasonicated for 15 min. $10\mu\text{L}$ of this dispersion was coated on glassy carbon electrode and $5\mu\text{L}$ of 5% styrene (as binder from Aldrich) was added on these coating and dried. The glassy carbon electrode was used as the working electrode and Ag/AgCl/KCl (saturated) was used as reference electrode. The cyclic voltammogram were recorded in acetonitrile using TBAP as electrolyte. The BET (Brunauer–Emmett–Teller) surface areas were determined with the use of

N₂ sorption data measured at 77 K with a volumetric adsorption setup (NOVA 1000e, Quantachrome Instruments). The pore diameters of the samples were determined from the desorption branch of the N₂ adsorption isotherm with the Barret, Joyner, and Halenda (BJH) method. The enantiomeric excess (ee) of the product was determined by HPLC (High Performance Liquid Chromatography) analysis using chiral columns (ϕ 4.6 mm x 250 mm, DAICEL CHIRALCEL OD-H or CHIRALPAK AD-H). CHNS/O-analyser, Perkin Elmer was used for elemental detection. Inductively Coupled Plasma (ICP) spectrometer analysis (Perkin Elmer, Model No. ICP Optima 2100 DV) and Atomic Absorption Spectroscopy (AAS, ICE 3500 Thermo Scientific) were used to detect % Cu in Cu²⁺-Y and Cu²⁺-Y-CD. The XPS measurements were made on a KRATOS (ESCA AXIS 165) spectrometer by using Mg K α (1253.6 eV) radiation as the excitation source. Charging of catalyst samples was corrected by setting the binding energy of the adventitious carbon (C 1s) at 284.6 eV. The finely ground oven-dried samples are dusted on a double stick graphite sheet and mounted on the standard sample holder. The sample holder is then transferred to the analysis chamber, which can house 10 samples at a time, through a rod attached to it. The samples are out gassed in a vacuum oven overnight before XPS measurements. ¹³C CP-MAS NMR measurements were performed on Bruker ultra-shield 500 MHz WB NMR spectrometer at 11.75 T field producing ¹³C Larmor frequency at 125.77 MHz. The samples were loaded in a 3.2 mm zirconia rotor and spinning speed was set at 10 KHz. The pulse width applied corresponding to an angle of $\pi/2$ for the ¹³C nuclei was 2.3 μ s and with a pulse delay of 3 s. The pulse sequence applied was the normal single pulse. The chemical shift reference for ¹³C spectrum was set at 77 MHz corresponding to CDCl₃ peak. The line broadening applied for all the spectra was 100 Hz. ²⁹Si Solid State NMR measurements were performed on Bruker ultra-shield 500 MHz WB NMR spectrometer with triple resonance mass probe at 11.75 T field producing ²⁹Si Larmor frequency at 99.36 MHz. The samples were loaded in a 3.2 mm zirconia rotor and spinning speed was set at 10 KHz. The pulse width applied corresponding to an angle of $\pi/2$ for the ²⁹Si nuclei was 4 μ s and with a pulse delay of 10 s. The pulse sequence applied was ZG normal single pulse. The line broadening applied for all the spectra was 100 Hz. ²⁷Al Solid State NMR measurements were performed on Bruker ultra-shield 500 MHz WB NMR spectrometer with triple resonance mass probe at 11.75 T field producing ²⁷Al Larmor frequency at 130.31 MHz. The samples were loaded in a 3.2 mm zirconia rotor and spinning speed was set at 10 KHz. The pulse width applied corresponding to

an angle of $\pi/2$ for the ^{29}Si nuclei was 4 μs and with a pulse delay of 10 s. The pulse sequence applied was ZG normal single pulse. The line broadening applied for all the spectra was 100 Hz. ^1H Solid State NMR measurements were performed on Bruker ultra-shield 500 MHz WB NMR spectrometer with triple resonance magic probe at 11.75 T field producing ^1H Larmor frequency at 500 MHz. The samples were loaded in a 3.2 mm zirconia rotor and spinning speed was set at 10 KHz. The pulse width applied corresponding to an angle of $\pi/2$ for the ^1H nuclei was 13.5 μs and with a pulse delay of 1 s. The pulse sequence applied was ZG30 normal single pulse. The line broadening applied for all the spectra was 100 Hz.

RESULTS AND DISCUSSION

Elemental and surface area analysis

Elemental analyses of $\text{Cu}^{2+}\text{-Y}$ and $\text{Cu}^{2+}\text{-Y-CD}$ were carried out by CHN, AAS and ICP analysis. CHN analysis was performed to determine the carbon, hydrogen and nitrogen content in the $\text{Cu}^{2+}\text{-Y-CD}$ complex. The amount of metal content in $\text{Cu}^{2+}\text{-Y}$ and $\text{Cu}^{2+}\text{-Y-CD}$ were predicted by AAS and ICP analysis. The results of the elemental analyses are presented in Table 1. The Si/Al ratio in zeolite-Y was found to be ~ 2.5 consistent with the previously reported values.¹⁶ The amounts of metal content in the $\text{Cu}^{2+}\text{-Y-CD}$ was found to be less than those of the copper exchanged NaY zeolite, $\text{Cu}^{2+}\text{-Y}$ indicating the involvement of Cu^{2+} in complex formation with (-) cinchonidine. CHN analyses were found to be consistent with the expected molecular formula $\text{Cu}^{2+}\text{-cinchonidine}$ complex. In particular the C/N ratio was found to be almost the same as that of cinchonidine. This gave strong evidence for the interaction of CD with $\text{Cu}^{2+}\text{-Y}$.

BET (Brunauer-Emmett-Teller) surface area analysis was conducted to determine the surface area of the neat-NaY, $\text{Cu}^{2+}\text{-Y}$ and $\text{Cu}^{2+}\text{-Y-CD}$. BET adsorption isotherms are comparatively shown in Figure 1 and the surface area, pore dimension values are given in Table 1 along with elemental analysis. Similar pattern of the BET-isotherms were observed for all the systems. BET surface areas, pore size and pore volume of $\text{Cu}^{2+}\text{-Y-CD}$ was found to be significantly less in comparison to neat NaY, Table 1. Such significant change in BET surface area can be attributed to the formation of the Cu-cinchonidine complex inside zeolite-Y.²⁸

Fourier transform Infrared (FTIR) spectroscopy and solid state NMR (SSNMR) analysis

FTIR spectrum for zeolite-Y, cinchonidine, $\text{Cu}^{2+}\text{-Y}$ and $\text{Cu}^{2+}\text{-Y-CD}$ are shown in the Figure 2. FTIR spectra of Na-Y and $\text{Cu}^{2+}\text{-Y}$ show strong zeolite lattice bands in the region 450-1200 cm^{-1} . The strong band in the region 1010-1100 can be attributed to the asymmetric stretching vibration

of (Si/Al)O₄ units.²³ The band in the region 1650 cm⁻¹ is due to lattice water molecules and that in the region 3500 cm⁻¹ is due to surface hydroxyl group,¹⁹ Figure 2a and 2b. Some shifting in the O-H stretching region was observed in case of metal-exchanged zeolite-Y indicating the exchanged of Cu²⁺ with zeolite-Y. Vibrational bands for cinchonidine were observed at 1635, 1590, 1509 and 1454 cm⁻¹, Figure 2c. In case of the Cu²⁺-Y supported cinchonidine, characteristic bands for cinchonidine were found at 1513 and 1461 cm⁻¹ Figure 2d. These bands were slightly shifted from that of neat cinchonidine due to the effect of zeolite matrix. The appearance of these two bands indicates the encapsulation of cinchonidine on Cu²⁺-Y.

D. Ferri and T. Bürgi reported that cinchonidine adsorbed on Pt/Al₂O₃ surface in three different ways one *via* π -system, by H-abstraction and one by the lone pair of nitrogen atom of quinoline ring.¹¹ To the best of our knowledge however, it is not reported for possible binding interaction of CD with zeolite-Y. Just like on adsorption of cinchonidine on platinum surfaces, there might occur various such possibility of interaction of CD with metal exchanged zeolites. First CD has two different types of rings, quinoline and quinuclidine and these two rings are free to rotate about C-C bond linking the two moieties. Quinoline ring is quite planar in nature and has a kinetic radius of $\sim 6.2 \text{ \AA}$ and can diffuse through the pores of zeolite-Y having diameter of $\sim 7.4 \text{ \AA}$. The measured average molecular dimensions of the double aromatic ring structure of quinoline are $8:42 \pm 0:8 \text{ \AA} \times 7:30 \pm 0:7 \text{ \AA} \times 1:04 \pm 0:1 \text{ \AA}$ (length \times breadth \times height). These values are consistent with the corresponding van der Waals dimensions of naphthalene ($8:12 \text{ \AA} \times 7:36 \text{ \AA} \times 3:4 \text{ \AA}$).²⁹ Therefore, there is a high possibility that the half of the cinchonidine molecule (the quinoline ring) can penetrate through the cavity of zeolite-Y. In other sense we can say such encapsulation as a case of *half-encapsulation* process, Scheme 1a. Quinuclidine ring of CD will get steric effect and hence will remain out of the cavity. In case of Cu²⁺ exchanged zeolite-Y recently Santra et al³⁰ from their theoretical study identified the location of Cu²⁺ site in zeolite-Y. The most probable sites are Site II and Site III. Adsorption on the other sites is less probable due to the preparation temperature of samples (below 773 K), at which copper does not migrate into the sodalite or hexagonal cages. So it can be assumed that N-atom of quinoline ring will bind to the Cu²⁺ located at Site II and forms a tetracoordinated Cu²⁺ site as shown in Scheme 1a. On the other hand rather than forming complex with copper, there is also probability that CD can directly get adsorbed on the external surface of zeolite-Y *via* H-bonding formation as shown in Scheme 1b. Further, acidic protons of zeolite-Y can protonate the N-atom of quinuclidine. From

FTIR spectral analysis it was evident that in case of CD interacting with Cu^{2+} -Y peaks were observed at 1513 and 1461 cm^{-1} apart from the vibrational bands of zeolite-Y. Usually vibrational bands within the region of 1200-1600 cm^{-1} indicates presence of metal complex in zeolite-Y.²³ The structure of the alkaloid cinchonidine is shown in Scheme 1c along with the spectral region of cinchonidine within 1650-1450 cm^{-1} . In the FTIR spectrum of cinchonidine vibrational modes of the vinyl ($\nu(\text{C}=\text{C})$) were observed at 1635 cm^{-1} . Quinoline ring modes were found at 1590 and 1509 cm^{-1} and quinuclidine at 1454 cm^{-1} . In the FTIR spectrum of Cu^{2+} -Y-CD bands were observed at 1637, 1513 and 1461 corresponding to vinyl ($\nu(\text{C}=\text{C})$), quinoline ring and quinuclidine moieties.¹¹ Thus presence of characteristics bands of cinchonidine indicates its interaction with zeolite-Y. Encapsulation of quinoline ring into the pores of zeolite-Y was found to be temperature dependent. Initially when we treated cinchonidine with zeolite-Y and stirred at room temperature for 24h, we could not find any characteristic bands of CD in the FTIR spectrum of Cu^{2+} -Y-CD. On heating the reaction mixture at 80 °C, we obtained the FTIR spectrum as shown in Figure 2d. Probably higher temperature favours the diffusion of CD to the cavity of zeolite-Y.

FTIR did not give any clear information regarding the interaction of CD with zeolite-Y. Further to confirm the interaction of CD with Cu^{2+} -Y we recorded the ^1H , ^{29}Si and ^{27}Al NMR. Solid-state NMR (SSNMR) appears to be a powerful technique for characterizing noncrystalline organic samples and also diamagnetic organometallic complexes.³¹ Due to low sensitivity/resolution and difficulties in ^1H decoupling associated with large paramagnetic shifts till now only a handful of SSNMR studies have been performed for paramagnetic organometallic complexes in rigid solids.³²⁻³⁵ Yoshitaka Ishii and his coworkers have however made a significant contribution in developing SSNMR techniques in characterizing paramagnetic metal complexes.^{36,37} ^1H NMR spectra of the Cu^{2+} -Y-CD shown in Figure 3a shows sharp peak at ~10 ppm and weak peak nearly at ~18 ppm. The presence of spinning sidebands indicated the presence of large dipolar anisotropy. The two observed peak can be attributed to the involvement of internal silanol OH with the aromatic proton of quinine ring. Signals for the H-atom of the zeolite-Y were masked by the paramagnetic environment. Since ^1H -NMR signals could not provide a better evidence regarding the interaction of CD with Cu^{2+} -Y, we record the ^{13}C NMR spectra of the immobilized system. ^{13}C NMR spectra recorded at 10 KHz spinning speed gave signal at 138.86, 114.72, 40.12 and 23.76 ppm close to the carbon atoms marked as

1, 2, 3 and 4 respectively in Figure 3b. These signals correspond to vinyl carbon atom and two of the carbon atoms of quinuclidine ring. Peaks corresponding to quinoline rings were not retrieved due to large paramagnetic effect imparted by Cu^{2+} ion. This analysis indicates that probably quinoline rings are inside the cavity of zeolite-Y whereas the rest part of CD could not diffuse inside the cavity due to steric hindrance associated with the quinuclidine moiety.

In the ^{29}Si -NMR recorded for Cu^{2+} -Y-CD peaks were observed at -99, -95, -94, -88 and -83 ppm, Figure 4a. In general -105 to -107 indicate Si (0Al) neighbour, -95 to -105 Si (1Al) -88 to -95 Si(2Al), -86 to -92 Si(3Al) and -80 to -86 Si(4Al).^{38,39} Thus the characteristic ^{29}Si NMR chemical shift observed in Cu^{2+} -Y-CD suggest for the presence of Si-O-Al linkage in zeolite framework. Slight change observed in ^{29}Si NMR chemical shift can be attributed to the effect of copper complex environment. Presence of sharp peak at 59 ppm in the ^{27}Al NMR spectra also clearly represents the tetrahedral arrangement of Al(IV) species in zeolite-Y, Figure 4b.^{38,40} Absence of peak at 0(zero) ppm indicates for the non-existence of the octahedral Al(VI) species.

Ultra violet-visible/ diffuse reflectance (uv-vis/dr) spectroscopy

UV-Vis spectrums of cinchonidine was recorded in solution phase whereas those for Cu^{2+} -Y and Cu^{2+} -Y-CD were measured in solid phase in reflectance mode (diffuse reflectance spectrum, DRS). In the UV-Vis spectrum of cinchonidine recorded in acetonitrile bands were found at 283, 301 and 314 nm, Figure 5a. The sharp intense band at 283 nm was due to $\pi \rightarrow \pi^*$ transition and band at 314 was because of $n \rightarrow \pi^*$ transition. The Cu^{2+} -exchanged zeolite-Y gave bands at 214 and 845 nm, Figure 5b. The band at 214 nm was due to charge transfer transition (LMCT) from O-atom of zeolite-Y to Cu^{2+} and that at 845 nm was due to d-d transition originated from the metal ion. For Cu^{2+} -Y supported cinchonidine bands were observed at 228, 312 and 721 nm, Figure 5c. The band at 228 and 312 nm corresponding to quinoline ring⁴¹ clearly indicates the attachment of quinoline ring of cinchonidine with Cu^{2+} -Y. Further, shifting of the d-d transition band by 133 nm and appearance of weak MLCT-band at 396 nm also confirms the involvement Cu^{2+} ion in bonding with N-atom of quinoline ring, Figure 5c.

X-ray photo electron spectroscopy (XPS)

Cu^{2+} -Y-CD complex was characterized by XPS analysis in order to confirm oxidation state of copper after immobilization of cinchonidine. XPS spectra of Cu^{2+} -Y and Cu^{2+} -Y-CD are shown in Figure 6a and Figure 6b, respectively. In both the system two intense principal peaks were

obtained at ($\text{Cu } 2p_{3/2}$ and $\text{Cu } 2p_{1/2}$) at 934.3 and 955.2 eV accompanied by a satellite peak at 942.3 eV.⁴² Presence of satellite peak nearly about 10 eV higher than the $\text{Cu } 2p_{3/2}$ confirmed +2 oxidation state of copper. N(1s) XPS spectrum of the Cu^{2+} -Y-CD complex is shown in Figure 7a. Two nitrogen peaks were found at 399.4 eV and 400.8 eV corresponding to N-atom of quinoline and quinclidine of cinchonidine, respectively.⁴³ K. Artyushkova et al.⁴⁴ has recently reported that N-atom bonded with metal shows signal $\sim 1\text{eV}$ less than the unbonded one. Since the energy separation between the two nitrogen atom in Cu^{2+} -Y-CD complexes is $\sim 1.4\text{eV}$ therefore it clearly indicates the co-ordination of cinchonidine with Cu^{2+} *via* quinoline N-atom. Figure 7b shows the C1s XPS spectrum of the Cu^{2+} -Y-CD complex. Four different peaks centred at 284.6, 285.8 and 288.1 eV were observed, corresponding to C=C, C-OH and C=N bonds, respectively of cinchonidine.^{43,45} Presence of characteristics peak in XPS spectra reveals the fact that cinchonidine is bonded to copper-exchanged zeolite-Y. XPS analyses are in good agreement with those observed by Lambert for cinchonidine supported on Pt surface.⁴³

Electrochemical studies

Information on the nature of the intrazeolite complexes can be obtained by cyclic voltammetry that may not be readily apparent from spectroscopic studies.⁴⁶ Cyclic Voltammogram of cinchonidine at a scan rate of 0.2 V/s is shown in Figure 8a. The CV did not exhibit any significant signal; however, some changes in current were observed. Cyclic voltammogram of Cu^{2+} -Y and Cu^{2+} -Y-CD were recorded as zeolite modified electrode (ZME). The CV of Cu^{2+} -Y Figure 8b resulted in one oxidation peak due to $\text{Cu(I)} \rightarrow \text{Cu(II)}$ process at 0.871 V and one reduction peak at 0.195 V because of $\text{Cu(II)} \rightarrow \text{Cu(I)}$ process. In case of Cu^{2+} -Y supported cinchonidine Figure 8c, the oxidation peak was observed at 0.744 V and two reduction peaks were observed at -0.398 V and -0.626 V. Difference in the redox potential values between Cu^{2+} -Y and Cu^{2+} -Y-CD can be attributed to the effect of binding of cinchonidine with Cu^{2+} -Y.

Powder X-ray diffraction and scanning electron microscope (PXRD and SEM) analysis

PXRD patterns of Cu^{2+} -Y and cinchonidine supported Cu^{2+} -Y-CD complex are shown in Figure 9. PXRD pattern for both the systems were found to be almost same except slight shifting in 2θ values. It indicates that the crystalline structure of zeolite-Y was well maintained after reacting with cinchonidine. SEM analysis also suggests that because of the immobilization of cinchonidine there occurs no change in surface morphology thereby maintains the heterogeneity

of the system, Figure 10. In the PXRD spectra of Cu^{2+} -Y-CD complex the intensity of (311) plane at 2θ value of 11.97 was found to be more than the corresponding Cu-exchanged zeolite-Y. The alternation of peak intensity clearly confirms the encapsulation of cinchonidine moiety in zeolite-Y cavity.^{23,47,48} This alternation of peak intensity was in accordance with PXRD pattern for zeolite-Y encapsulated complexes reported by various other researchers.

Asymmetric Henry reaction using Cu^{2+} -Y-CD as catalyst

Cinchonidine and its derivatives are well known to act as chiral auxiliaries in various asymmetric reactions.⁸⁻¹⁰ Recently, Hammar et al⁴⁹ has performed DFT based calculation to understand the mechanism of asymmetric Henry reaction using cinchona thiourea as chiral catalyst. Various metal exchanged zeolites or zeolite-Y encapsulated complexes are also known to catalyzed nitro-aldol reaction.²³ So we opt to perform asymmetric Henry reaction using our chirally modified heterogeneous catalyst. While performing the reaction we considered the effect of solvent, temperature and amount of catalyst. Taking 4-nitrobenzaldehyde as a test substrate we screened various solvent systems and found acetonitrile (CH_3CN) as suitable solvent, Table 2. It is pertinent to mention herein that we have excluded the use of polar solvent like water and alcohols in order to prevent additional H-bond-donor or -acceptor abilities from the polar, aprotic solvents.⁹ On reacting for 48h and at ice cool condition (measured to be 4°C) we obtained highest 86% yield and 72% ee of the S-product in acetonitrile in presence of Cu^{2+} -Y-CD complex. Comparison with neat NaY and Cu^{2+} -Y catalyst, Cu^{2+} -Y-CD catalyst gives better yield and enantioselectivity. This indicates co-ordination of (-) cinchonidine enhances the catalytic activity and results in significant enantioselectivity. In order to study the effect of temperature we choose a range of temperature from room temperature (32°C) to -40°C . To see these affects we performed the nitro-aldol reaction taking 4-nitrobenzaldehyde as test substrate and Cu^{2+} -Y-CD complex as catalyst in acetonitrile. The results obtained are given in Table 3. At -4°C the percentage yield of the reaction was high 94% with 88% ee. Below this or above this temperature % yield and % ee were not so significant. This might be due to the fact that at or above -4°C the reaction conditions were not so favored for the formation of the suitable transition states or the intermediates states. To understand the effect of amount of catalyst on the catalytic conversion, we first choose five different amounts of the catalyst (0.05g, 0.10g, 0.15g, 0.20g and 0.25g) keeping the substrate concentration fixed. The effect of variation of catalytic

amount was carried out using 4-nitrobenzaldehyde, which was taken as a test substrate. The increase in the amount of catalyst from 0.05 to 0.15g tremendously increases the catalytic conversion from 38-86% yield and gave 72% ee at ice cool temperature. However, the percentage yield was found to be less on increasing the amount of catalyst from 0.20 to 0.25g and other side products were obtained as minor product. So we choose 0.15g catalyst as the optimum concentration and performed the catalytic conversion with different aldehydes. After optimizing the suitable reaction condition (solvent: CH₃CN, temperature:-4°C and catalyst amount: 0.15g) we carried out nitro-aldol reaction using nitromethane and a range of aldehydes. Results of these investigations using Cu²⁺-Y-CD complex are given in Table 4. The nitro-aldol products were characterized by ¹H and ¹³C NMR and FTIR analysis (see supporting information). Aldehydes with an electron withdrawing group were found to give high enantioselectivity and better productivity. Reactants with electron donating groups and with more aromatic ring gave low yield and reduced the enantioselectivity. This might be due to the fact that presence of electron withdrawing group makes the aldehydic carbon centre more susceptible for the nucleophilic attack. In the HPLC analysis, we obtained two isomers (*S*-major and *R*-minor). The absolute configuration of the nitro aldol products were assigned by comparison of the retention time with the reported literature (see supporting information).^{50,51} Based on these results it can be said that the synthesized Cu²⁺-Y-CD complex can be used as a heterogeneous chiral catalyst for enantioselective Henry reaction.

Compared to the previous results, the catalytic activity of this catalyst is more or less comparable. Lai et al.⁵² reported for 99% ee and yield for nitro-aldol product using Cu-tertiary amine complex with different aldehydes. Xiong et al.⁵³ obtained 95% yield and more than 90% ee with 4-nitrobenzaldehyde using copper (I) Schiff-base complex. Bisoxazoline Cu(II) complex reported by Evans et al.⁵⁴ was also found to be excellent chiral catalyst for asymmetric Henry reaction giving more than 95% yield and enantioselectivity. Although there are several copper based chiral homogeneous catalysts reported for catalyzing such kind C-C coupling reaction⁵⁴ but to best of our knowledge very few heterogeneous chiral catalysts are reported. From our group we recently found Cu-Schiff base complex encapsulated in zeolite-Y as good reusable chiral catalyst for Henry reaction.^{23,42} Khan et al. also obtained more than 90% yield and %ee in nitro-aldol product using Cu-Schiff base complex encapsulated in ZSM-5 and NaY zeolite.⁵⁵ Maggi et al.⁵⁶ evaluated that a polystyrene-supported chiral BOX/copper complex (a

heterogeneous catalyst) can promote Henry reaction with enantioselectivity of the nitro-aldol product upto 88%. Besides these reports lanthanum-lithium-BINOL chiral complex covalently linked to MCM- 41 mesoporous silica polythiophene salen-chromium complex derivatives,⁵⁷ chiral BOX copper complex immobilized onto magnetically separable mesoporous silica and chiral diamines linked to zeolites were also found to be suitable chiral catalyst for asymmetric Henry reaction. Hence, based on previous reports it can be said Cu^{2+} -Y-CD catalyst reported herein giving more than 90% yield and 88% ee can be a beneficial and useful chiral heterogeneous catalyst and can contribute to the field of asymmetric catalysis.⁵⁷⁻⁶²

Hammar et al⁴⁹ proposed that nitro-aldol reaction with cinchonidine proceeded with the abstraction of a proton from nitromethane by the quinuclidine N-atom. In order to confirm the fact we simply react our catalyst with nitromethane and then recorded the ¹H NMR. We observed a broad signal at 15.34 ppm (Figure 11) which matches with the previously reported by D. M. Meier et al.⁶³ They also observed a broad signal nearly at 14.8 ppm due to protonation of the quinuclidine N-atom of CD. This result further substantiate the fact that quinuclidine ring gets protonated and thereby generates the nitronate ion (CH_2NO_2^-) during the course of nitro-aldol reaction. Based on this NMR analysis we have proposed a plausible mechanism for the asymmetric Henry reaction. A schematic representation for the same is provided in Scheme 2. Probably, in the first step as said above a proton from nitromethane get abstracted by the quinuclidine N-atom generating a nitronate ion. In a simultaneously process aldehyde molecules passed through the channels of zeolite-Y and in the supercage C-C coupling process occurs as shown in Scheme 2. Nitronate ion, however before undergoing C-C coupling reaction first gets bonded to the Cu^{2+} and then attack the aldehydic carbon atom. Once the C-C coupling products formed it gets diffused from the cavity and finally abstracts the proton from quinuclidine N-atom. During this process the product gets chirally induced because of the chiral environment created by the cinchonidine moiety, Scheme 2

Recyclability test

We could successfully performed the nitro-aldol reaction for two consecutive cycles without any loss in enantioselectivity. But after the two cycles the catalytic results were found to be very poor. In order to get insight of the loss of catalytic activity we again characterized the recovered catalyst by FTIR, ²⁹Si and ²⁷Al NMR. FTIR spectrum of the recovered catalyst was found to be completely different from the parent complex, Figure 12a and Figure 12b. Comparison of the

FTIR spectra in the region of 3200-4000 cm^{-1} and 1000-1600 cm^{-1} with that of the initial catalyst is shown respectively in Figure 13 a and Figure 13b. From both the figures it is clearly observed that in case of the catalyst recovered after two cycles large number of bands are present above 3200 cm^{-1} . Presence of such vibrational bands in the H-bonding region indicates that probably the cinchonidine moiety get detached from the metal centre and remains on the external surface of zeolite-Y. Bands above 3500 cm^{-1} also confers for H-bonding interaction between silanol group and cinchonidine moiety as shown in Scheme 1b.⁶⁴ ^{29}Si and ^{27}Al NMR were also found to differ from the initial catalyst, Figure 14a and Figure 14b, respectively. Numbers of multiplets were observed in ^{29}Si NMR spectra indicating that Si surrounded by various Al species in crystalline manner and also by non crystalline domains. ^{27}Al NMR of the recovered catalyst shows peak at 52.20 ppm which is upfield by 7 ppm in comparison to parent catalyst. Thus it is evident from the spectrochemical studies that cinchonidine no longer remains bonded to Cu-centre and thereby affects the uniform heterogeneity of the system leading to catalytic deactivation.

Theoretical calculations

Density functional theory (DFT) calculations were performed using Gaussian 09 programme.⁶⁵ The calculations were performed using B3LYP functional and 6-31+G** basis set. The zeolite cluster that we considered in this study was generated by taking a 42-atom cluster with the initial atom positions for all Si (Al) and O atoms taken to be those for siliceous faujasite. Initially, the framework Si and O atoms of the clusters were held fixed at their crystallographic positions and all the terminal H atoms were optimized. Following the Löwenstein rule two silicon atoms in the framework was exchanged with two aluminium atoms to incorporate one Cu^{2+} ion. The gas phase optimized cinchonidine molecule was then interacted with Cu^{2+} -exchanged zeolite-Y at different orientation. While optimizing the clusters, terminated hydrogen atoms were held fixed at their initially optimized positions. The most stable structure was considered for further analysis.

The optimized geometries of cinchonidine, Cu^{2+} -Y and Cu^{2+} -Y-CD complex are shown in Figure 15. The C-C, C=N, C-H and O-H bond lengths in cinchonidine molecules were found to be in good agreement with the expected one. In both the systems Cu^{2+} -Y and Cu^{2+} -Y-CD metal ion (Cu^{2+}) was found to be located just above the plane of the six-membered O-ring. Al-O, Cu-O, Cu-Si and Cu-Al distances in the considered clusters are listed in Table 5. The average

distances were found to match well with those reported for similar kind of Cu-exchanged zeolite-Y.⁶⁶ However, on interaction with the cinchonidine the Cu-O, Cu-Si and Cu-Al were found to slightly elongated from the parent Cu²⁺-Y, Table 5 which may be due to steric impartment imposed by the ligand system. The Cu-N(quinoline) bond distance in Cu²⁺-Y-CD complex was found to be 1.99 Å indicating the possibility of strong co-ordinate bond between copper and cinchonidine.

We have also calculated the HOMO and LUMO energies of the cinchonidine and Cu²⁺-Y-CD complex. In both the cases HOMO was found to concentrate at quinuclidine ring while LUMO was found to concentrate at the quinoline ring, Figure 16. But the energy of the HOMO in case of cinchonidine was found to be -0.221 a.u. while in case of Cu²⁺-Y-CD it was found to be -0.243 a.u. Similarly, energy of LUMO in cinchonidine was found to be -0.065 a.u. while in Cu²⁺-Y-CD it was found to be -0.128 a.u. This clearly indicates that on interacting with Cu-exchanged zeolite-Y the frontier orbitals of cinchonidine becomes more stabilized in comparison to free cinchonidine molecule. The interaction energy between the Cu²⁺-Y and cinchonidine molecule was found to be -243 kcal/mol.

Conclusions

Copper exchanged zeolite-Y is chirally modified with cinchonidine. Adsorption of cinchonidine or coordination of cinchonidine with Cu²⁺-Y is confirmed by various spectroscopic tools. Encapsulation of cinchonidine is believed to occur *via* thermal diffusion process. Solid state NMR and XPS analysis confirms that quinoline moiety of cinchonidine remains bonded with copper in interior cavity of zeolite-Y while rest of the moiety remains outside the cavity due to steric hinderance. Cinchonidine modified copper exchanged zeolite-Y serves as an excellent chiral catalyst in asymmetric Henry reaction. About 88% of enantiomeric excess has been achieved in the nitro-aldol product using this chiral catalyst. Chiral catalyst was used for two consecutive cycles without any loss in enantioselectivity. But the catalyst activity was found to get diminished due to detachment of the cinchonidine moiety from the copper centre after two cycles.

Acknowledgements

KKB thanks Science and Engineering Research Board, (SERB), Department of Science and Technology (DST), India for the financial grant (NO SB/EMEQ-463/2014)

Supporting information

¹H, ¹³CNMR and HPLC analysis of nitro-aldol products, complete reference of Gaussian 09.

Contact Author: kusum@tezu.ernet.in

References

- 1 Y. Orito, S. Imai, S. Niwa, *Nippon Kagaku Kaishi*, 1979, **8**, 1118-1120.
- 2 R. L. Augustine, K. T. Setrak, L. K. Doyle, *Tetrahedron Asymm.*, 1993, **4**, 1803-1827.
- 3 P. B. Wells, A. G. Wilkinson, *Top. Catal.*, 1998, **5**, 39-50.
- 4 H.-U. Blaser, H.-P. Jalett, M. Garland, M. Studer, H. Thies, A. Wirth-Tijana, *J. Catal.*, 1998, **173**, 282-294.
- 5 J. Wang, Y.-K. Sun, C. LeBlond, R. N. Landau, D. G. Blackmond, *J. Catal.*, 1996, **161**, 752-758.
- 6 Y. K. Sun, J. Wang, C. LeBlond, R. N. Landau, D. G. Blackmond, *J. Catal.*, 1996, **161**, 759-765.
- 7 C. Le Blond, J. Wang, A. T. Andrews, Y.-K. Sun, *Top. Catal.*, 2000, **13**, 169-174.
- 8 T. Mallat, E. Orglmeister, A. Baiker, *Chem. Rev.*, 2007, **107**, 4863 -4890.
- 9 F. Meemken, A. Baiker, S. Schenker, K. Hungerbuhler, *Chem. Eur. J.*, 2014, **20**, 1298-1309.
- 10 F. Meemken, A. Baiker, J. Dupre, K. Hungerbuhler, *ACS Catal.*, 2014, **4**, 344 -354.
- 11 D. Ferri, T. Bürgi, *J. Am. Chem. Soc.*, 2001, **123**, 12074-12084.
- 12 N. A. Rey, K. C. dos Santos, M. Â. B. C. Menezes, A. S. Mangrichc, E. C. P. Maia, *J. Braz. Chem. Soc.*, 2006, **17**, 497-504.
- 13 Q. M. Xu, D. Wang, L. J. Wan, C. L. Bai, Y. Wang, *J. Am. Chem. Soc.*, 2002, **124**, 14300-14301.
- 14 R. A. Olsen, D. Borchardt, L. Mink, A. Agarwal, L. J. Mueller, F. Zaera, *J. Am. Chem. Soc.*, 2006, **128**, 15594-15595.
- 15 D. J. Xuereb, R. Raja, *Catal. Sci. Technol.*, 2011, **1**, 517-534.
- 16 J. M.; Thomas, R. Raja, *Acc. Chem. Res.*, 2008, **41**, 708-720.
- 17 K. K.; Bania, D.; Bharali, B. Viswanathan, R. C. Deka, *Inorg. Chem.*, 2012, **51**, 1657-1674.
- 18 A. Corma, H. Garcia, *Eur. J. Inorg. Chem.*, 2004, 1143-1164.
- 19 I. Ogino, B. C. Gates, *J. Am. Chem. Soc.*, 2008, **130**, 13338-13346.
- 20 F. Blatter, H. Frei, *J. Am. Chem. Soc.*, 1994, **116**, 1812-1820.

- 21 A. Uzun, B. C. Gates, *J. Am. Chem. Soc.*, 2009, **131**, 15887–15894.
- 22 D. G. Lahr, J. Li, R. J. Davis, *J. Am. Chem. Soc.*, 2007, **129**, 3420-3425.
- 23 K. K. Bania, G. V. Karunakar, K. Goutham, R. C Deka, *Inorg. Chem.*, 2013, **52**, 8017-8029.
- 24 N. Herron, D. R. Corbin, *Inclusion Chemistry with Zeolites: Nanoscale Materials by Design*, Kluwer Academic Publisher, **1995**
- 25 N. Herron: *Zeolite Catalysts as Enzyme Mimics*, *ACS Symp. Ser.*, 1989, **392**, 141-154.
- 26 U. Böhmer F. Franke, K. Morgenschweis, T. Bieber, W. Reschetilowski, *Catal. Today*, 2000, **60**, 167-173.
- 27 T. Bein, P. Enzel, *Angew. Chem.*, 1989, **28**, 1692-1694.
- 28 S. Seelan, A. K. Sinha, D. Srinivas, S. Sivasanker, *J. Mol. Catal. A: Chem.*, 2000, **157**, 163-171.
- 29 D. Dahlgren, J. C. Hemminger, *Surf. Sci.*, 1982, **114**, 459-470.
- 30 S. Santra, T. Archipov, A. B. Ene, H. Komnik, H. Stoll, E. Roduner, G. Rauhut, *Phys.Chem.Chem.Phys.*, 2009, **11**, 8855-8866.
- 31 C. V. Grant, V. Frydman, J. S. Harwood, L. Frydman, *J. Am. Chem. Soc.*, 2002, **124**, 4458-4462.
- 32 V. P. Chacko, S. Ganapathy, R. G. Bryant, *J. Am. Chem. Soc.*, 1983, **105**, 5491 -5492.
- 33 A. N. Clayton, C. M. Dobson, C. P. Grey, *J. Chem. Soc., Chem. Commun.*, 1990, **72**-74.
- 34 T. P. Spaniol, A. Kubo, T. Terao, *Mol. Phys.*, 1999, **96**, 827-834.
- 35 K. Liu, D. Ryan, K. Nakanishi, A. McDermott, *J. Am. Chem. Soc.*, 1995, **117**, 6897-6906.
- 36 Y. Ishii, P. Nalinda, P. N. Wickramasinghe, S. Chimon, *J. Am. Chem. Soc.*, 2003, **125**, 3438-3439.
- 37 P. N. Wickramasinghe, M. Shaibat, Y. Ishii, *J. Am. Chem. Soc.*, 2005, **127**, 5796-5797.
- 38 J. Jiao, W. Wang, B. Sulikowski, J. Weitkamp, M. Hunger, *Micropor. Mesopor. Mat.*, 2006, **90**, 246–250.
- 39 J. Klinowski, J. M. Thomas, C. A. Fyfe, G. C. Gobbi, J. S. Hartman. *Inorg. Chem.*, .1983, **22**, 63-66.
- 40 J. Rocha, J. Klinowski, *J. Chem. Soc., Chem. Commun.*, 1991, 1121-1122.
- 41 Q. An, Q. Chen, W. Zhu, Y. Li, C.; an Tao, H. Yang, Z.;Li, J. Wan, H. Tianc, G. A Li, *Chem. Commun.*, 2010, **46**, 725–727.
- 42 K. K. Bania, G. V. Karunakar, B. Sarma, R. C Deka, *ChemPlusChem*, 2014, **79**, 427-438.

- 43 J. M. Bonello, R. M. Lambert, *Surf. Sci.*, 2002, **498**, 212-228.
- 44 K. Artyushkova, B. Kiefer, B. Halevi, A. K. Gericke, R. Schloglc, P. Atanassov, *Chem. Commun.*, 2013, **49**, 2539-2541.
- 45 X. Zhong, J.; Jin, S.; Li, Z.; Niu, W.; Hu, R.; Li, J. Ma, *Chem. Commun.*, 2010, **46**, 7340-7342.
- 46 B. R. Shaw, K. E. Creasy, C. J. Lanczycki, J. A. Sargeant, M. Tirhado, *J. Electrochem. Soc.* 1988, **135**, 869-876.
- 47 W. H. Quayle, J. H. Lunsford, *Inorg. Chem.*, 1982, **21**, 97-103.
- 48 W. H. Quayle, G. Peeters, G. L. DeRoy, E. F. Vansant, J. H. Lunsford, *Inorg. Chem.*, 1982, **21**, 2226-2231.
- 49 P. Hammar, T. Marcelli, H. Hiemstra, F. Himoa, *Adv. Synth. Catal.*, 2007, **349**, 2537-2548.
- 50 G. Blay, L. R. Domingo, V. H. Olmos, J. R. Pedro, *Chem. Eur. J.*, 2008, **14**, 4725-4730.
- 51 S. Selvakumar, D. Sivasankaran, V. K. Singh, *Org. Biomol. Chem.*, 2009, **73**, 3156-3162.
- 52 G. Lai, F. Guo, Y. Zheng, Y. Fang, H. Song, K. Xu, S. Wang, Z. Zha, Z. Wang. *Chem. Eur. J.*, 2011, **17**, 1114 -1117
- 53 Y. Xiong, F. Wang, X. Huang, Y. Wen, X. Feng. *Chem. Eur. J.*, 2007, **13**, 829 -833.
- 54 D. A. Evans, D. Seidel, M. Rueping, H. W. Lam, J. T. Shaw, C. W. Downey. *J. Am. Chem. Soc.*, 2003, **125**, 12692-12693.
- 55 S. Selvakumar, D. Sivasankaran, V. K. Singh, *Org. Biomol. Chem.*, 2009, **7**, 3156-3162.
- 56 N. H. Khan, Md. B. Ansari, E. A. Prasetyanto, H. Jin, S.E. Park. *Tetrahedron: Asymmetry*, 2011, **22**, 117-123.
- 57 R. Maggi, D. Lanari, C. Oro, G. Sartori, L. Vaccaro. *Eur. J. Org. Chem.*, 2011, 5551-5554
- 58 A. P. Bhatt, K. Pathak, R. V. Jasra, R. I. Kureshy, N. u. H. Khan, S. H. R. Abdi, *J. Mol. Catal. A*, 2006, **244**, 110-117.
- 59 A. Zulauf, M. Mellah, E. Schulz, *J. Org. Chem.*, 2009, **74**, 2242-2245.
- 60 A. Zulauf, M. Mellah, E. Schulz, *Chem. Commun.*, 2009, 6574-6576.
- 61 J.-M. Lee, J. Kim, Y. Shin, C.-E. Yeom, J. E. Lee, T. Hyeon, B. M. Kim, *Tetrahedron: Asymmetry*, 2010, **21**, 285-291.
- 62 M. D. Jones, C. J. Cooper, M. F. Mahon, P. R. Raithby, D. Apperley, J. Wolowska, D. Collison, *J. Mol. Catal. A*, 2010, **325**, 8-14.

- 63 M. Daniel, A.; Urakawa, N.; Turra, H.; Rügger, A. Baiker, *J. Phys. Chem. A*, 2008, **112**, 6150-6158.
- 64 S. Das, S. P. Mahanta, K. K. Bania, *RSC Adv.*, 2014, **4**, 51496-51509.
- 65 M. C. Frisch, et al. Gaussian 09, revision A.1; Gaussian, Inc.: Wallingford, CT, 2009. Gaussian 09, Revision **A.1**, (complete reference is given in supporting information).
66. I. J. Drake, Y. Zhang, D. Briggs, B.Lim, T. Chau, A. T. Bell, *J. Phys. Chem. B* 2006, **110**, 11654-11664.

Table 1. Pore size, pore volume and surface area of NaY, Cu²⁺-Y, Cu²⁺-Y-CD obtained from BET analysis. Percentage of C,H and N are calculated from CHN analysis. %Cu loading is calculated from ICP analysis. % Cu loading obtained from AAS are shown in parenthesis.

Compound	Cu-Loading (mg/100mg)	BJH pore size (Å)	Pore volume (cm ³ /g)	BET surface area (m ² /g)	Elemental Analysis (%)		
					C	H	N
NaY	-	6.2	0.30	645	-	-	-
Cu ²⁺ -Y	13.82(13.08)	6.0	0.26	630			
Cu ²⁺ -Y-CD	7.53(12.45)	3.7	0.19	382	27.04	3.10	3.32
Cinchonidine	-	-	-	-	77.52	7.53	9.52

Table 2. Nitroaldol reaction of 4-nitrobenzaldehyde catalysed by NaY, Cu²⁺-Y and Cu²⁺-Y-CD in different solvent under ice cool condition. The values shown in parenthesis are amount isolated product in gram scale.

Solvent	Time(h)	NaY		Cu ²⁺ -Y		Cu ²⁺ -Y-CD	
		% Yeild	%ee	% Yeild	%ee	% Yeild	%ee
Toluene	48	-	-	-	-	-	-
CycloHexane	48	-	-	-	-	-	-
DCM	48	16(0.17)	-	47(0.49)	-	57(0.60)	20
Chloroform	48	18(0.19)	-	54(0.57)	-	68(0.72)	48
Acetonitrile	48	28(0.30)	-	58(0.61)	-	86(0.91)	72
Acetonitrile/DCM	48	25(0.26)	-	55(0.58)	-	78(0.82)	63
Chloroform/Acetonitrile	48	20(0.21)	-	48(0.50)	-	70(0.74)	58

Table 3. Effect of temperature on nitro-aldol reaction of 4-nitrobenzaldehyde taken as case study using Cu²⁺-Y-CD catalyst. The values shown in parenthesis are amount isolated product in gram scale.

Entry	Temp ^f (°C)	Solvent	Time(hr)	(%)Yield	(%) ee
1	32	acetonitrile	48	48 (0.50)	30
2	0	acetonitrile	48	90 (0.95)	80
3	-4	acetonitrile	48	94(0.99)	88
4	-10	acetonitrile	48	82(0.86)	64
5	-20	acetonitrile	48	76(0.80)	48
6	-30	acetonitrile	48	74(0.78)	45
7	-40	acetonitrile	48	67(0.71)	36

Table 4. Henry reaction of nitromethane with various aldehydes at -4 °C in presence of Cu²⁺-Y-CD catalyst. The values shown in parenthesis are amount of substrate and isolated product in gram scale.



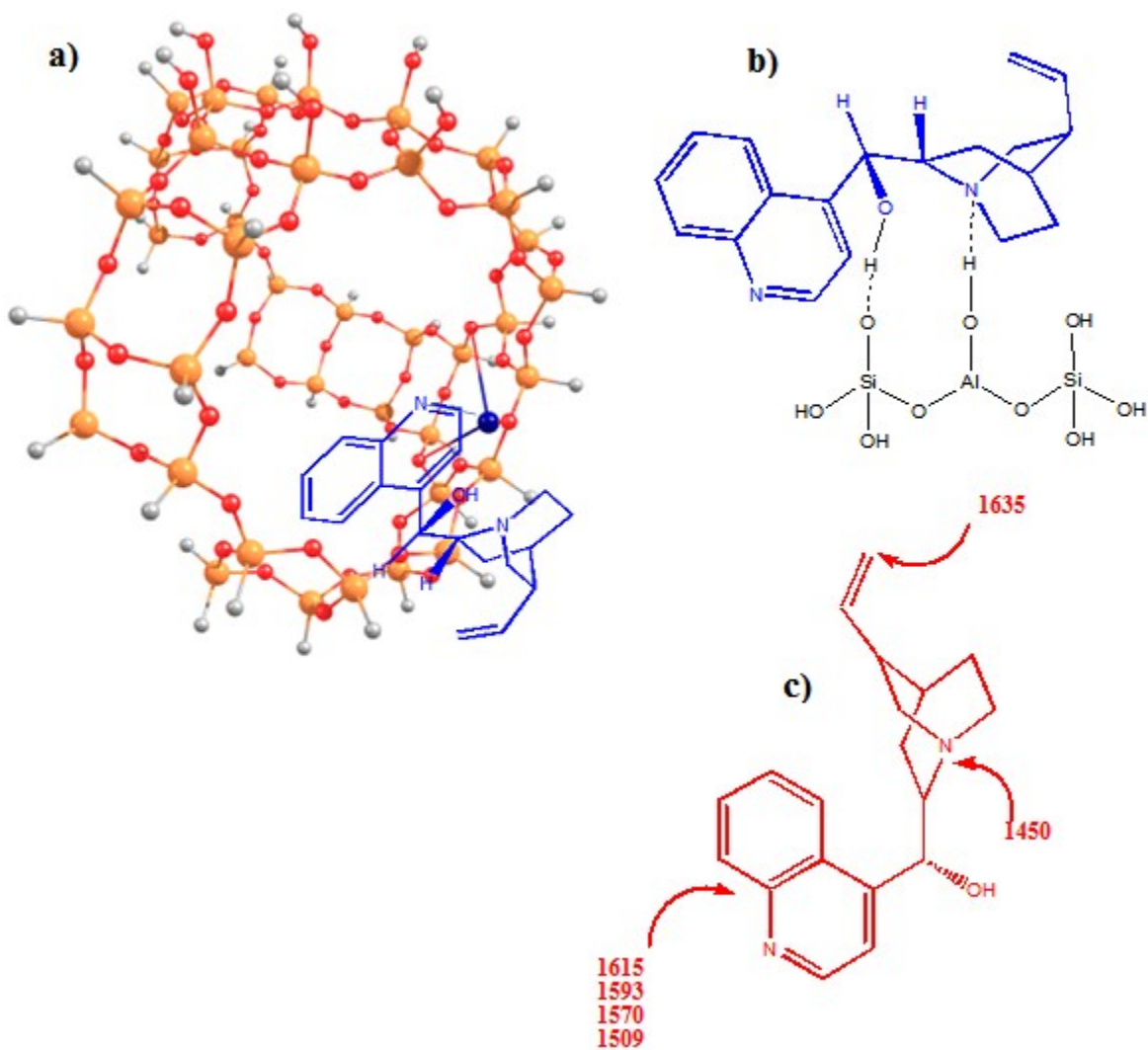
1a R₁= H, R₂ = H
 1b R₁= H, R₂ = NO₂
 1c, R₁= NO₂, R₂= H
 1d, R₁= H, R₂= CH₃
 1e, R₁=H R₂= OH
 1f, Naphthaldehyde

2a R₁= H, R₂ = H
 2b R₁= H, R₂ = NO₂
 2c, R₁= NO₂, R₂= H
 2d, R₁= H, R₂= CH₃
 2e, R₁=H R₂= OH
 2f, N1-(naphthalen-6-yl)-2-nitroethanol

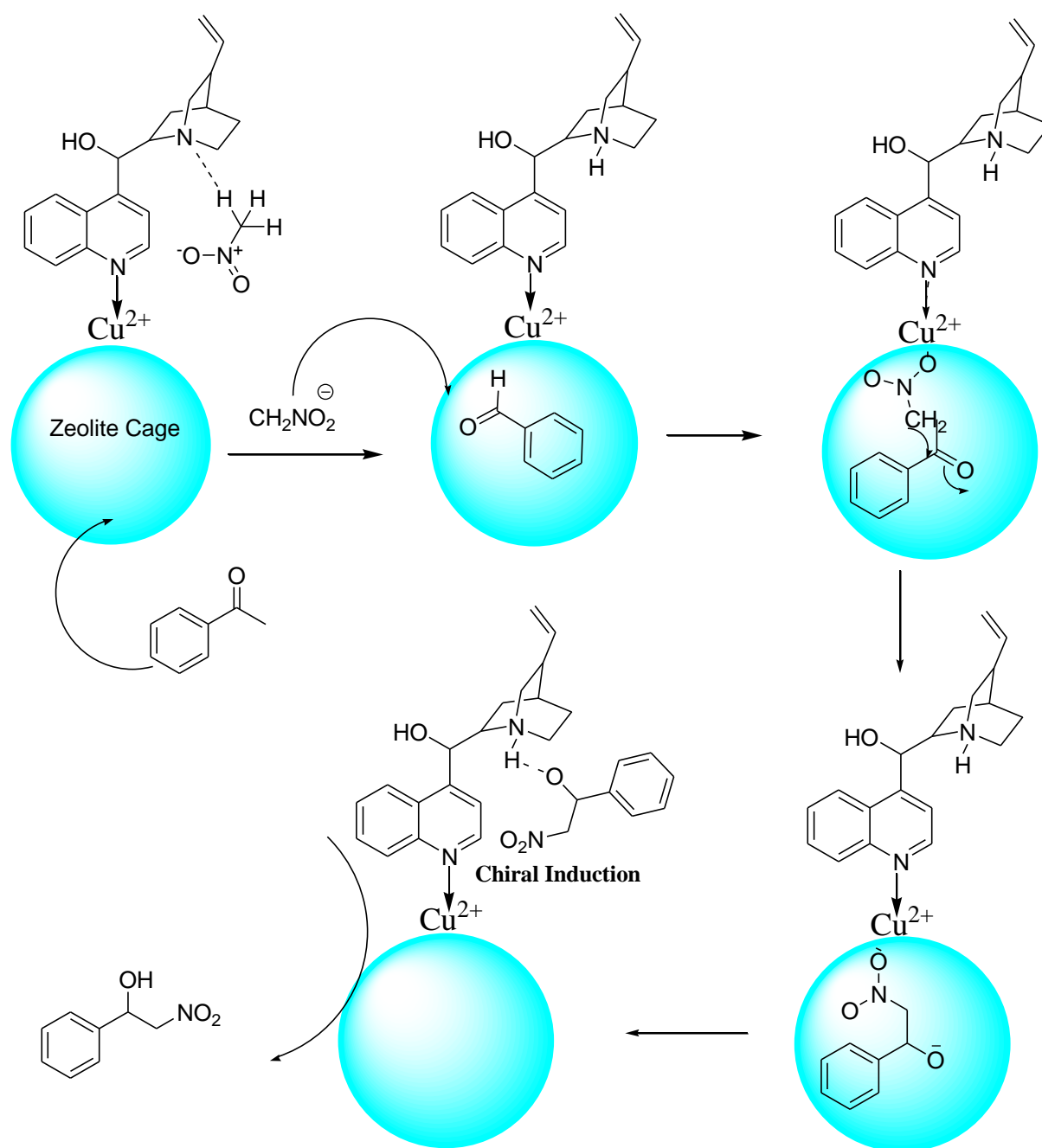
Substrate	Product	% Yield	Cofig ⁿ	%ee
1a(0.53)	2a	92(0.76)	S	78
1c(0.75)	2c	90(0.95)	S	84
1d(0.60)	2d	87(0.78)	S	72
1e(0.61)	2e	76(0.69)	S	68
1d(0.78)	2d	70(0.75)	S	65

Table 5. Bond distances (in Å) calculated from DFT calculation in the two model systems.

Model Systems	Cu-O	Cu-Al	Cu-Si	Al-O
Cu ²⁺ -Y	1.95	2.67	3.31	1.80
	2.34	3.15	3.17	1.74
	1.95		3.06	1.76
	3.37		3.03	1.69
	2.08			
	3.06			
Cu ²⁺ -Y-CD	2.02	2.83	3.42	1.83
	2.04	3.36	3.33	1.75
	1.97		3.37	1.77
	2.29		2.72	1.72
	3.37			
	3.61			



Scheme 1. a) and b) are probable interaction mode of cinchonidine with Cu²⁺-exchanged zeolite-Y. a) represents a half encapsulation process and b) represents interaction of cinchonidine with external zeolite surface. c) shows the selective vibrational bands in cinchonidine.



Scheme 2. A plausible reaction mechanism of the Henry reaction catalyzed by Cu²⁺-Y-CD complex

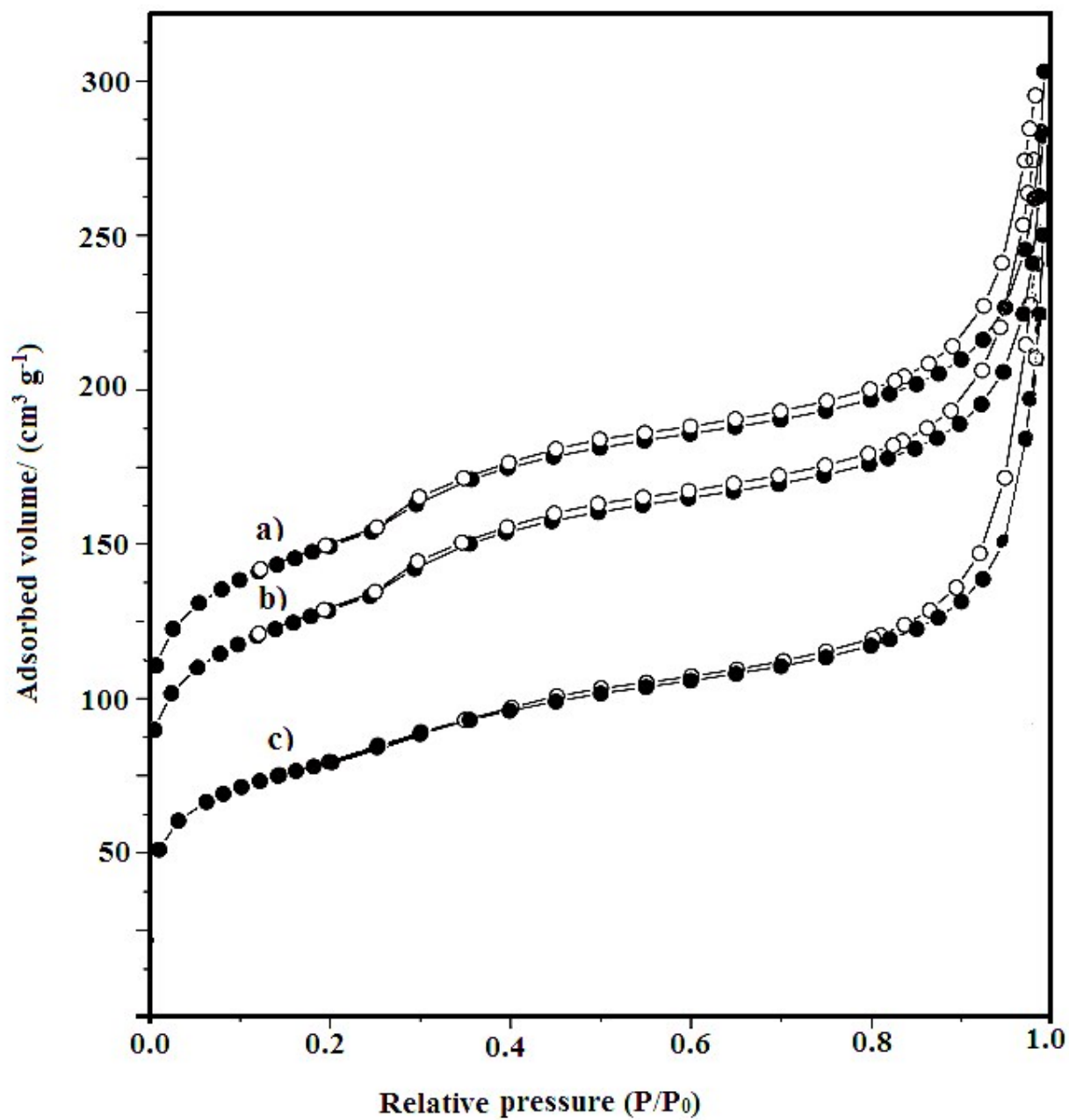


Figure 1. BET isotherms for a) NaY-zeolite b) Cu²⁺-exchnaged zeolite-Y c) Cu²⁺-Y-CD complex

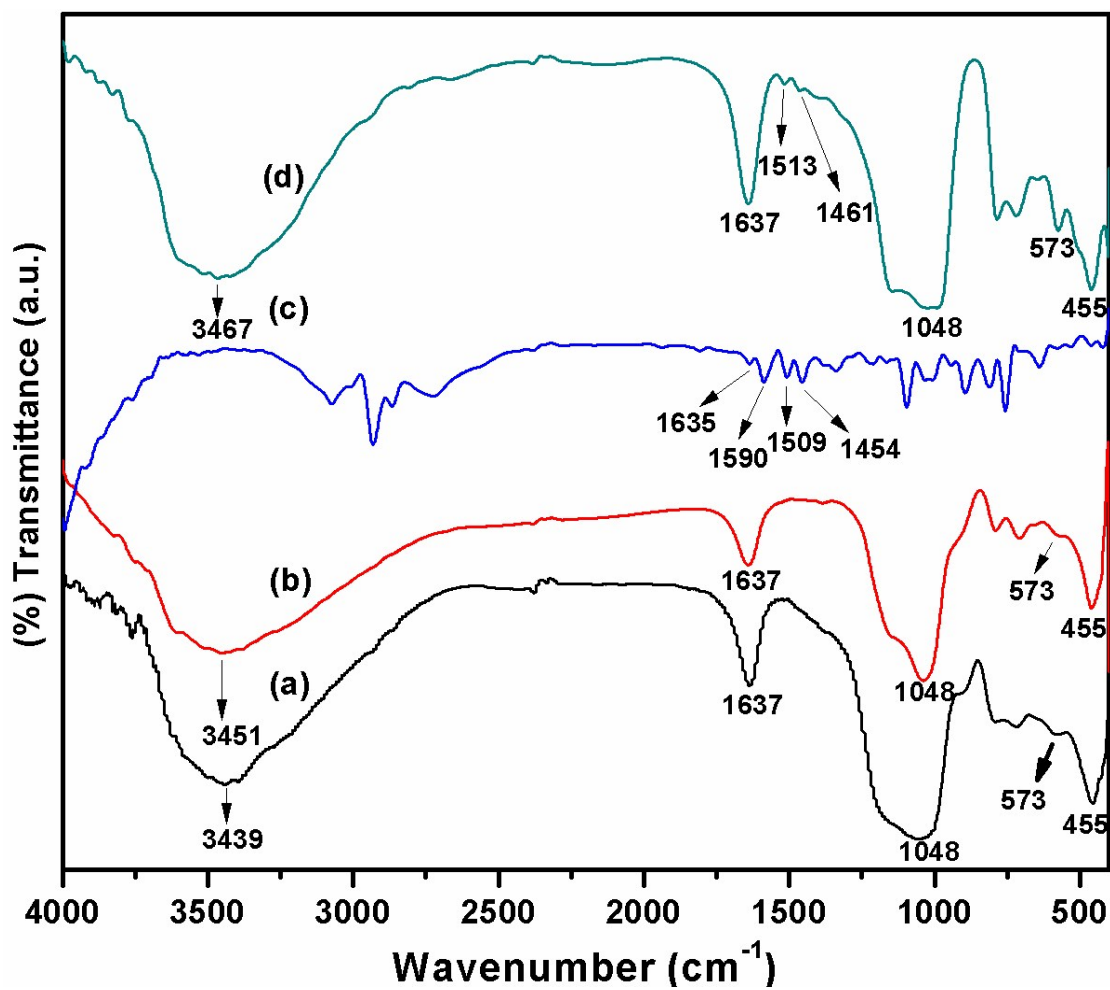


Figure 2: FTIR spectrum of (a) Zeolite-Y (b) Cu²⁺-Y (c) Cinchonidine, (d) Cu²⁺-Y supported cinchonidine

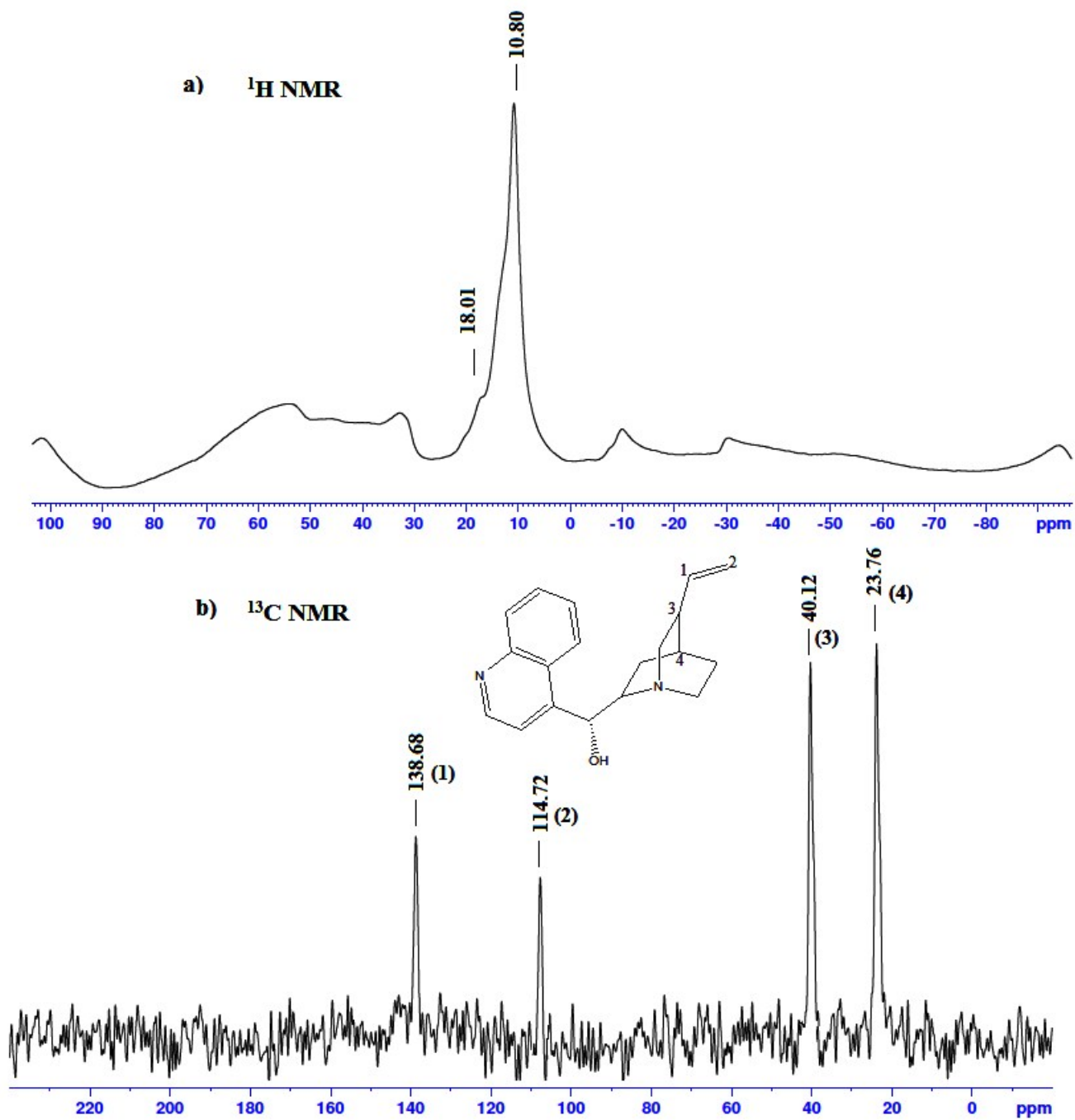


Figure 3. a) ^1H and b) ^{13}C NMR of Cu^{2+} -Y-CD complex

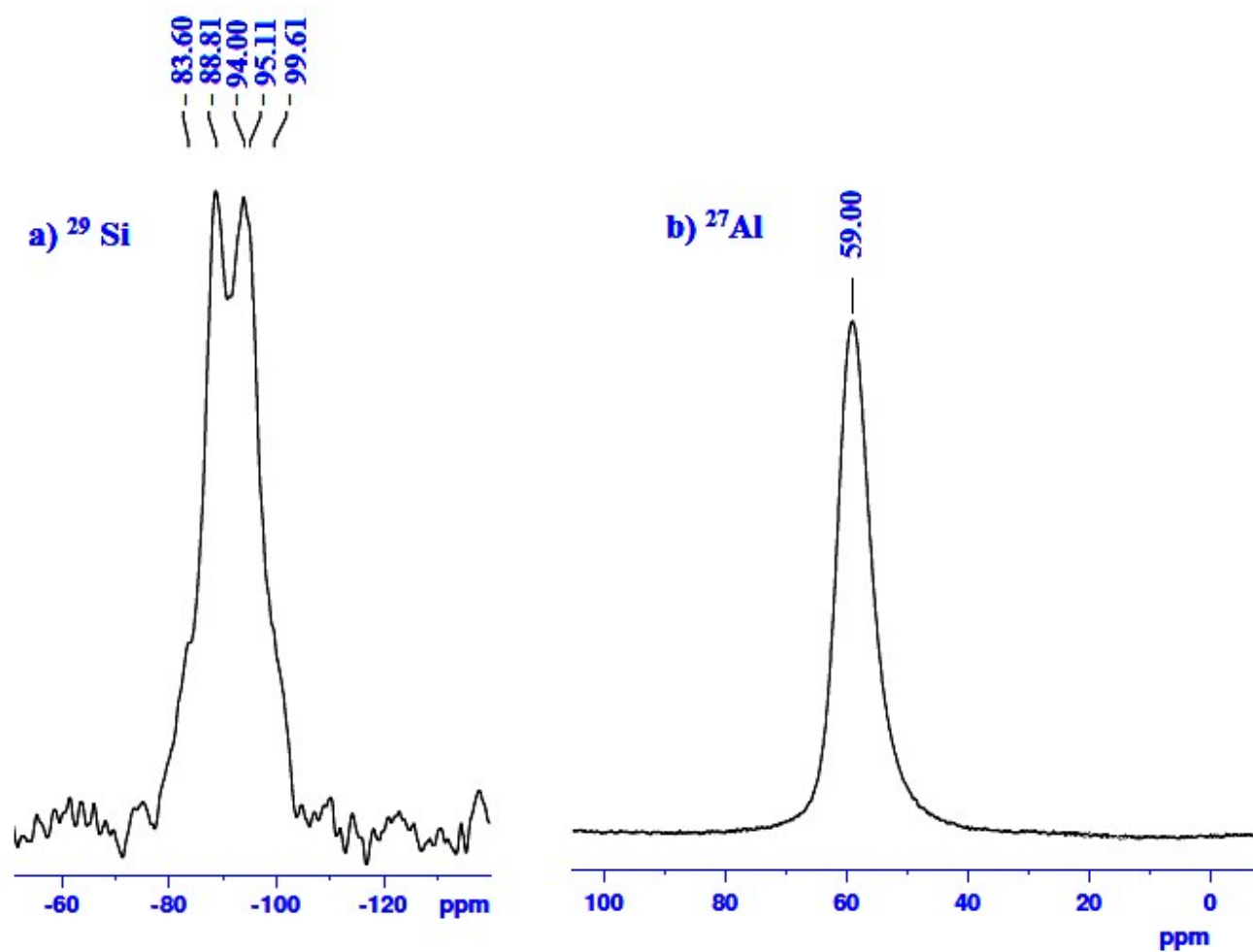


Figure 4 a) ^{29}Si NMR b) ^{27}Al NMR of Cu^{2+} -Y-CD complex

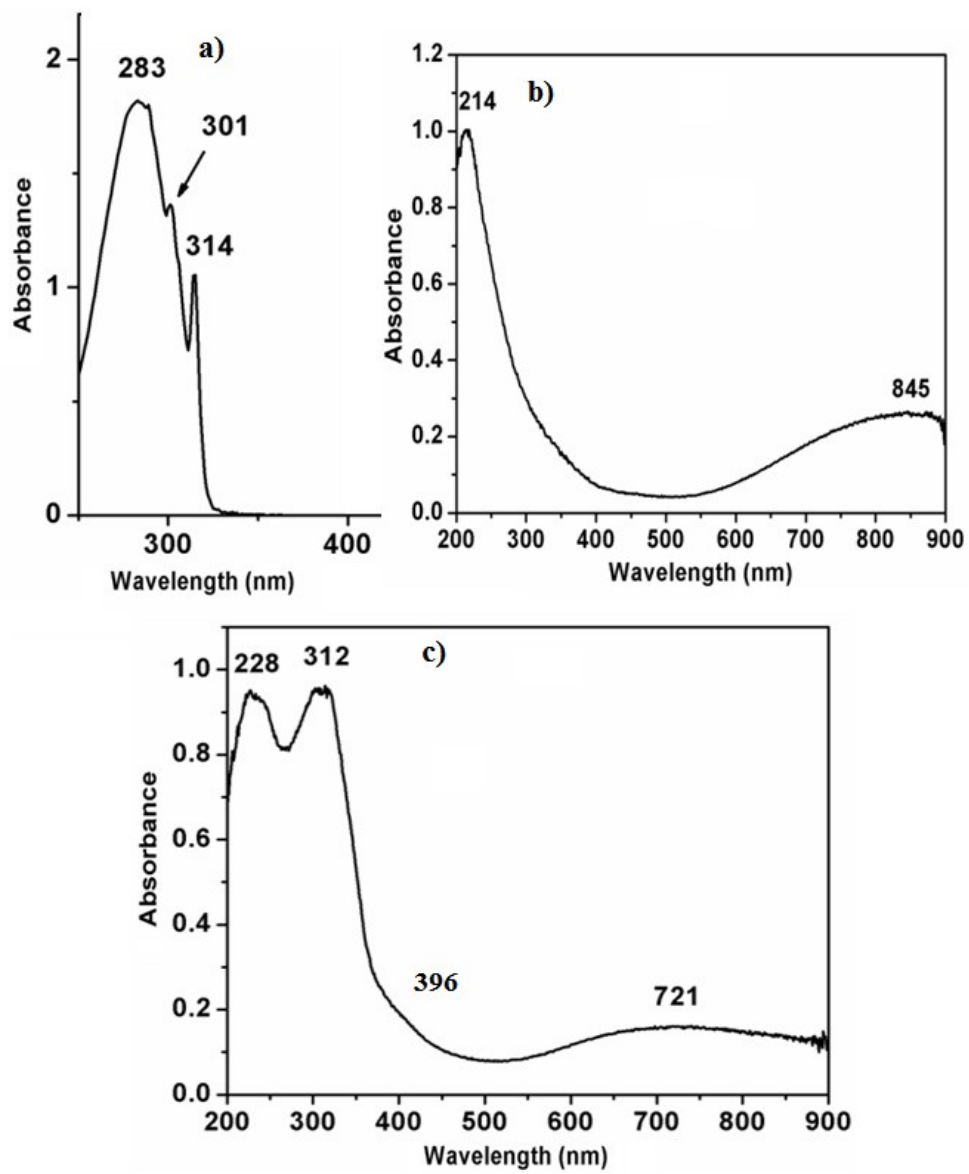


Figure 5. UV-Vis spectrum of a) cinchonidine (a) Cu^{2+} -Y, (b) Cu^{2+} -Y-CD

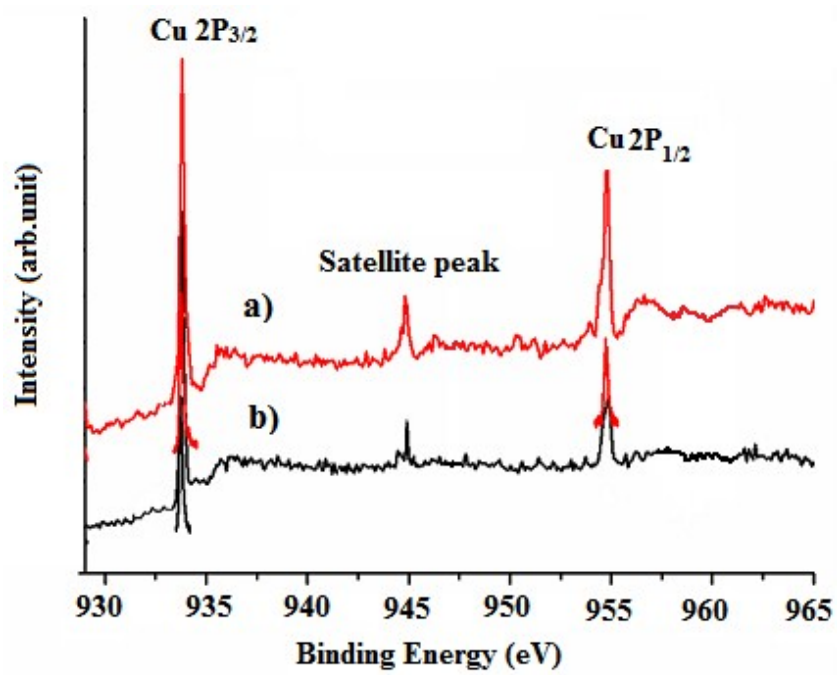


Figure 6. Cu(2p) XPS spectra of (a) Cu²⁺-Y, (b) Cu²⁺-Y-CD

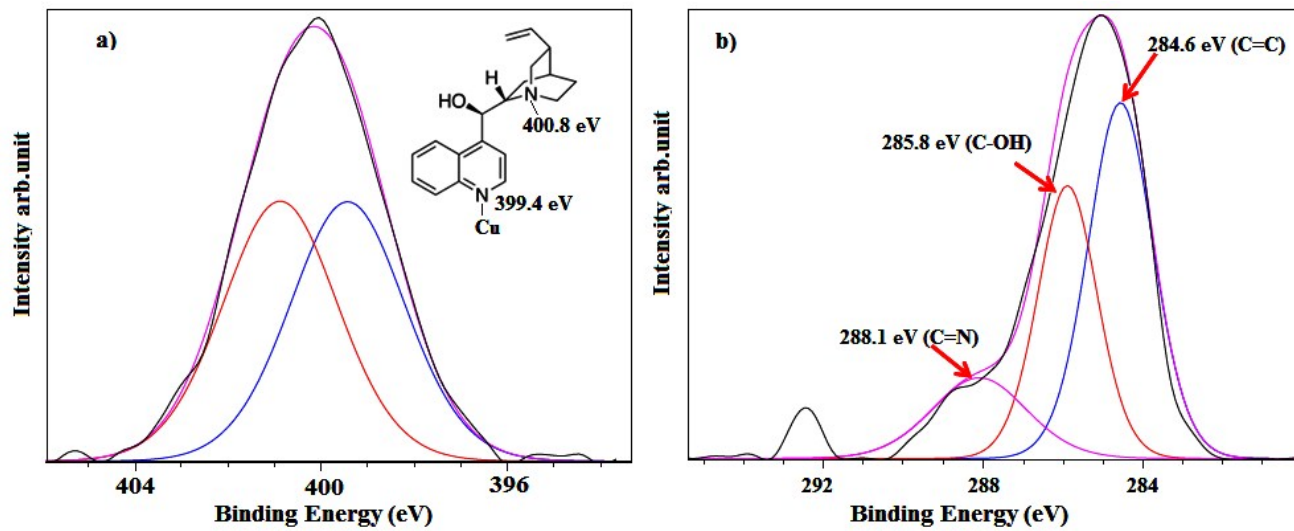


Figure 7 a) N(1s)-XPS spectra b) C(1s) XPS spectra of Cu²⁺-Y-CD complex

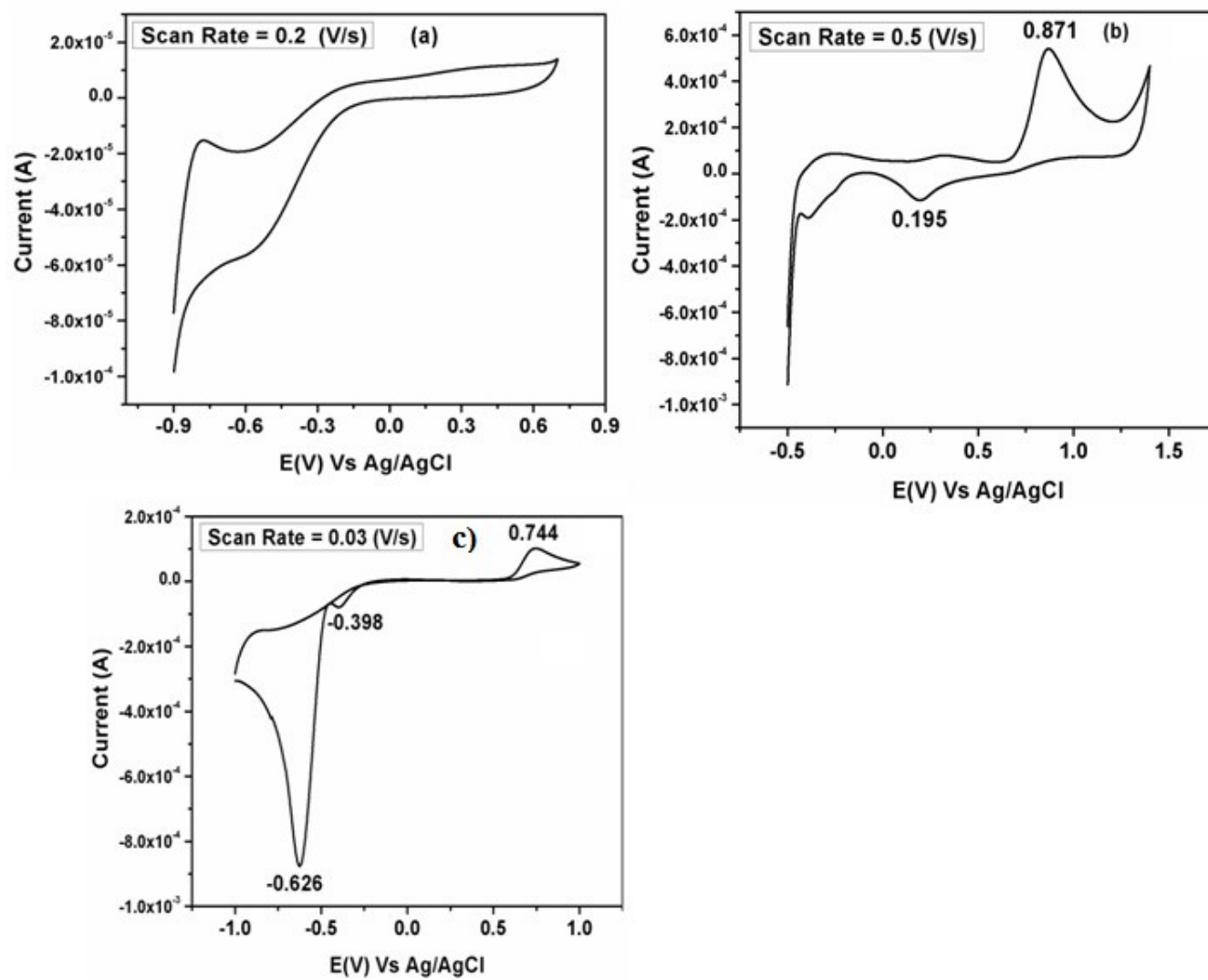


Figure 8. Cyclic voltammogram of a) cinchonidine (b) Cu^{2+} -Y, (c) Cu^{2+} -Y-CD

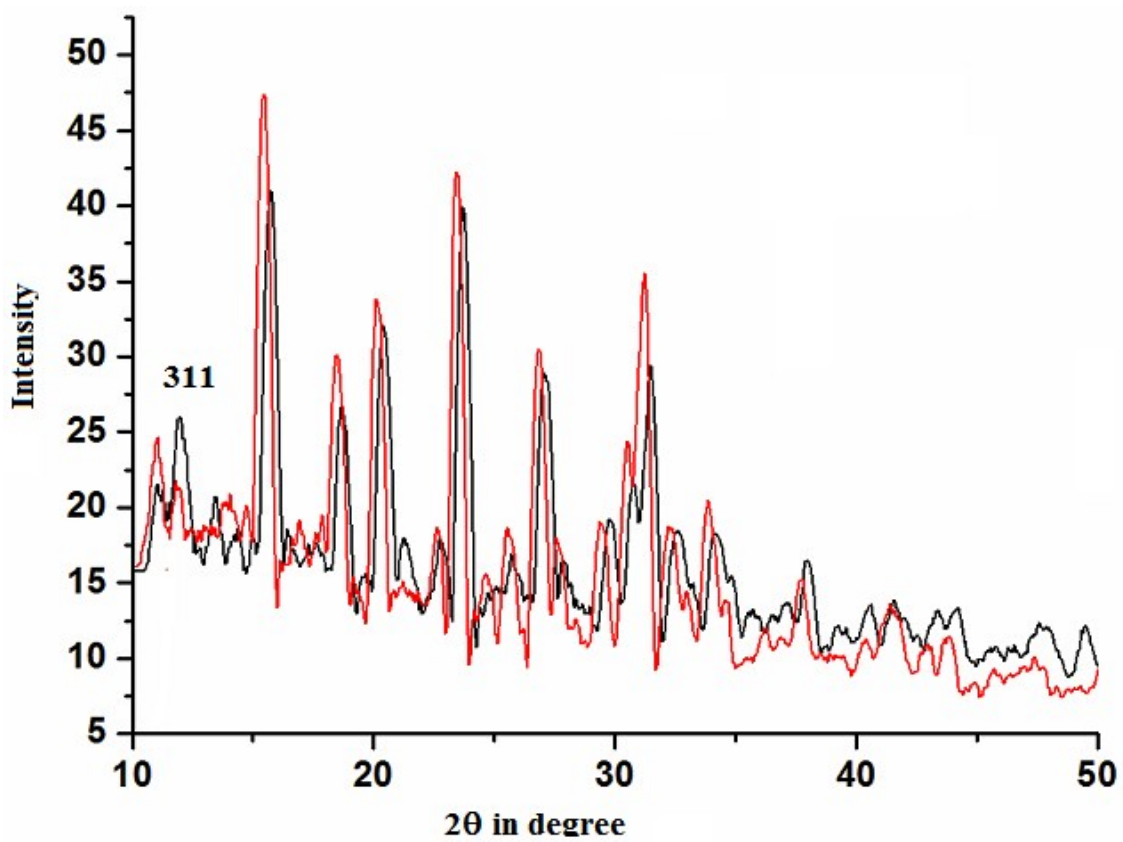


Figure 9. PXRD pattern of (a) Cu²⁺-Y(red) (b) Cu²⁺-Y-CD(black)

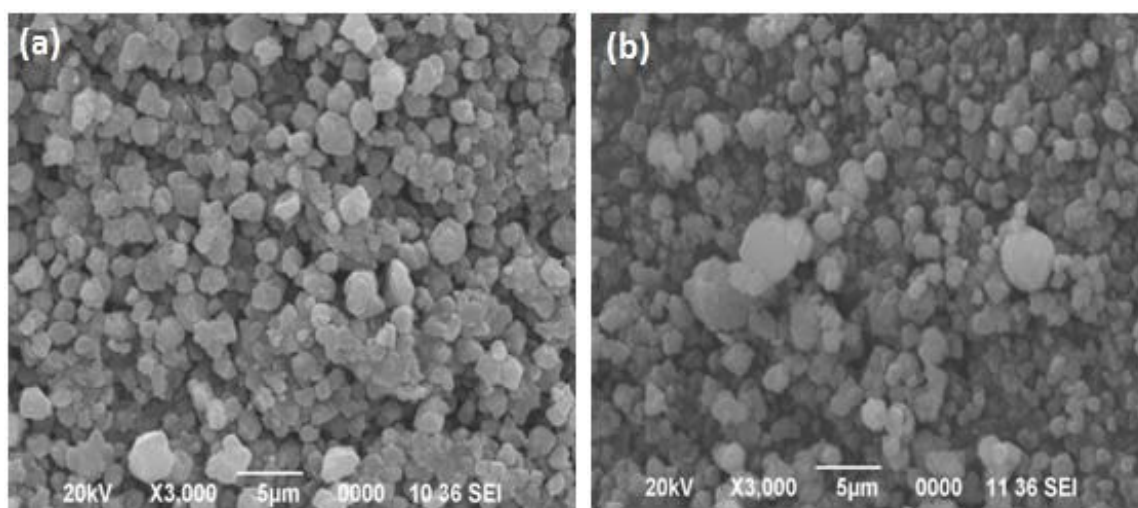


Figure 10. SEM image of (a) Cu^{2+} -Y, (b) Cu^{2+} -Y-CD

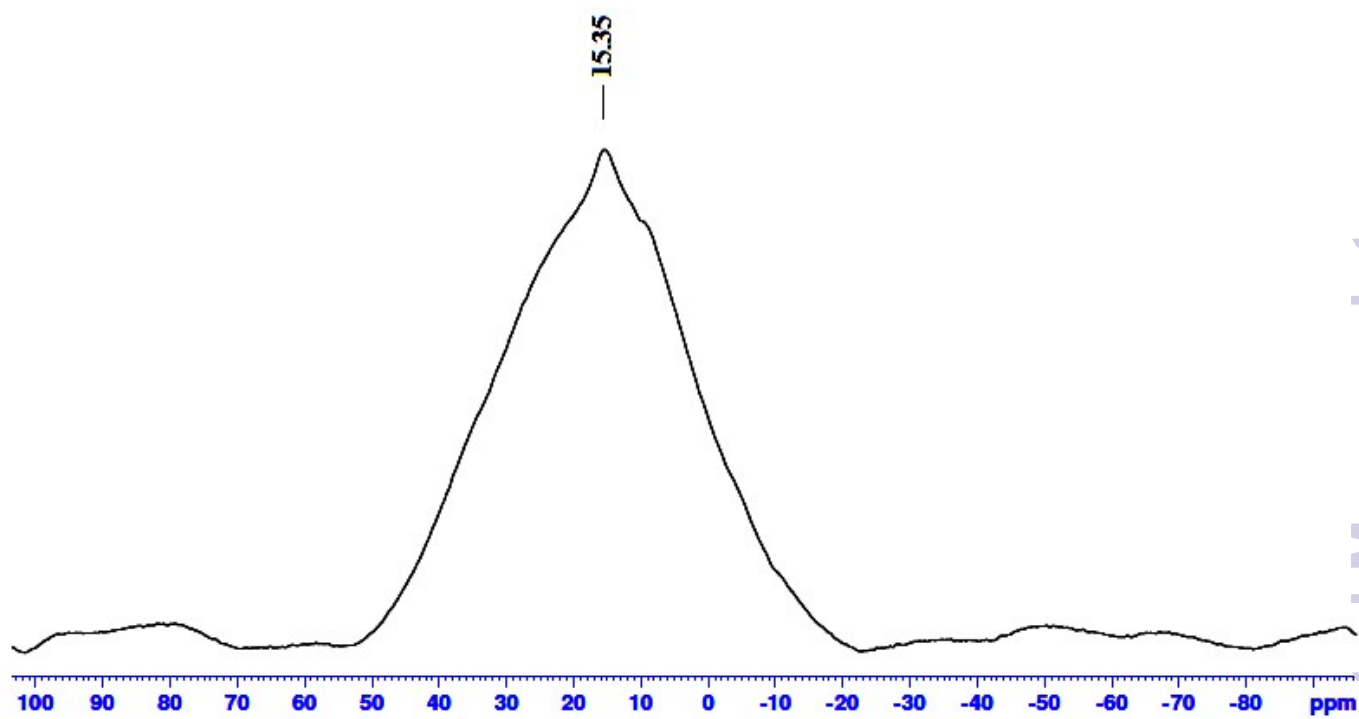


Figure 11. ^1H NMR spectra recorded after treatment of nitromethane with Cu^{2+} -Y-CD

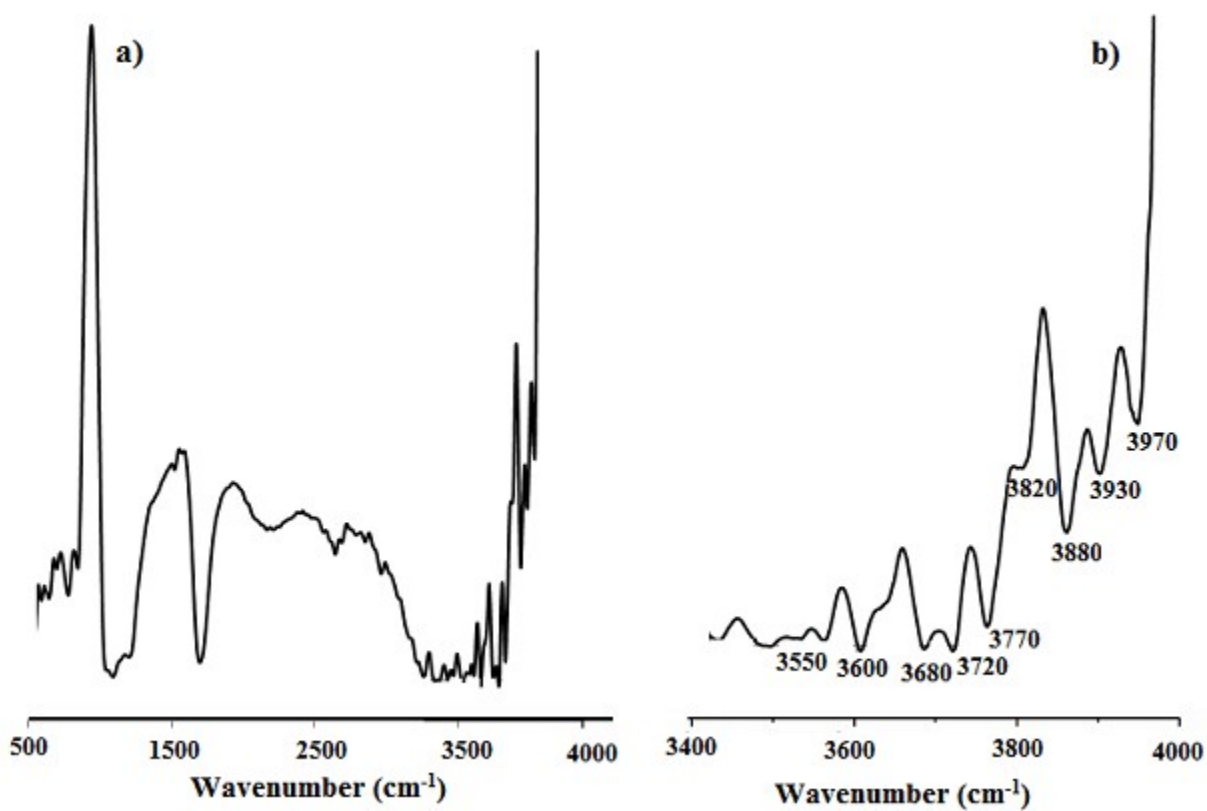


Figure 12. FTIR spectra of a) recovered Cu²⁺-Y-CD catalyst after two cycles b) recovered Cu²⁺-Y-CD catalyst in the region of 3400-4000 cm⁻¹

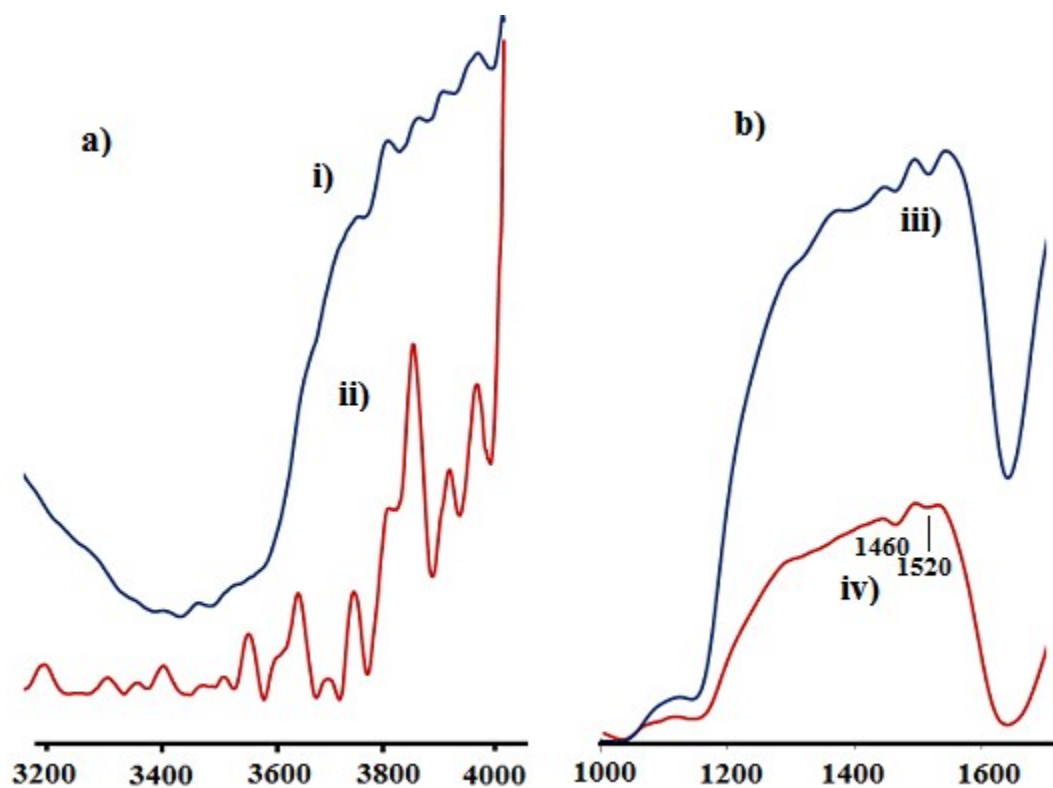


Figure 13. a) Comparison FTIR spectra of a) i) initial Cu^{2+} -Y-CD catalyst ii) recovered Cu^{2+} -Y-CD catalyst after two cycles in the region of 3200-4000 cm^{-1} b) i) initial Cu^{2+} -Y-CD catalyst ii) recovered Cu^{2+} -Y-CD catalyst after two cycles in the region of 1000-1600 cm^{-1} .

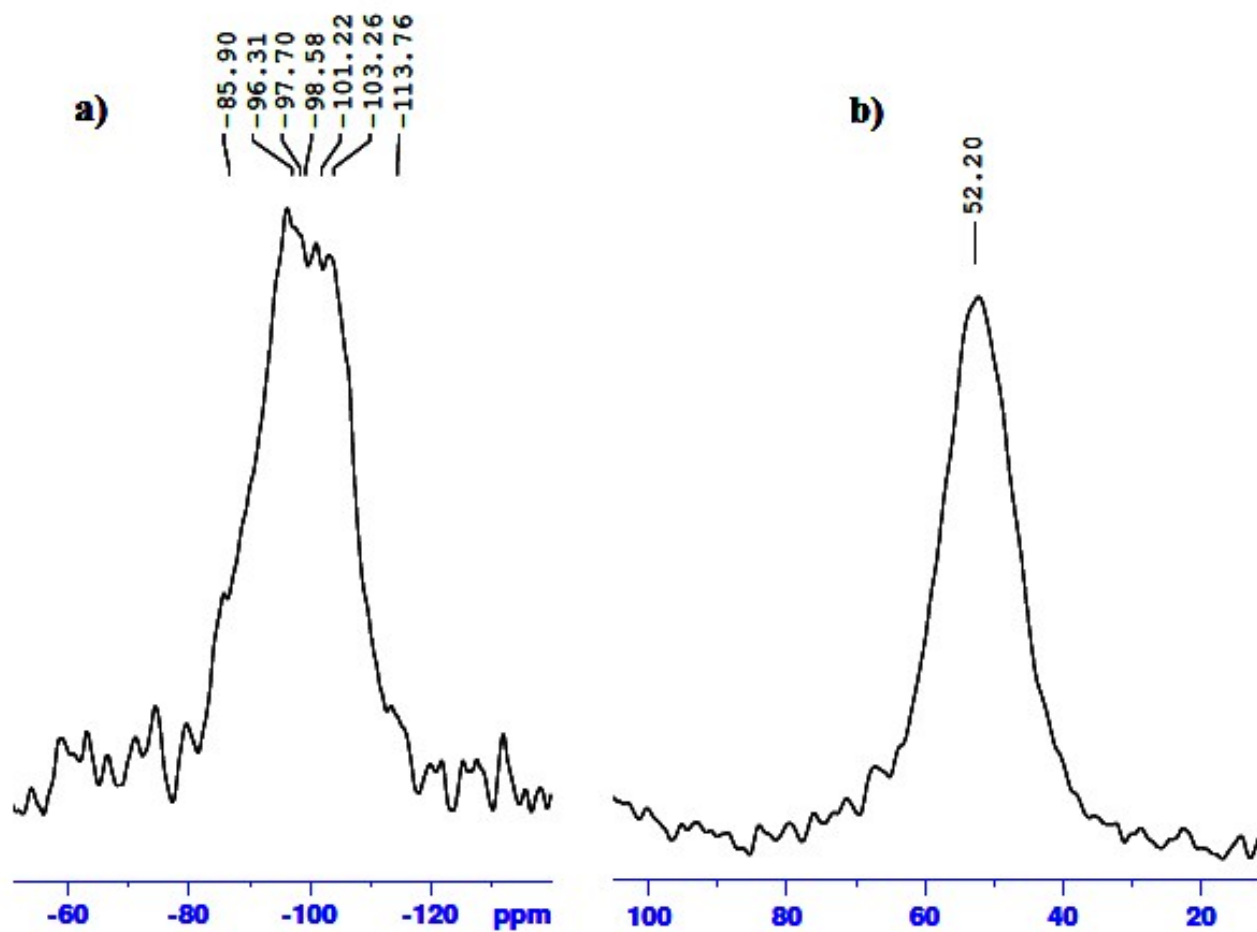


Figure 14. a) ^{29}Si NMR b) ^{27}Al NMR of recovered Cu^{2+} -Y-CD catalyst

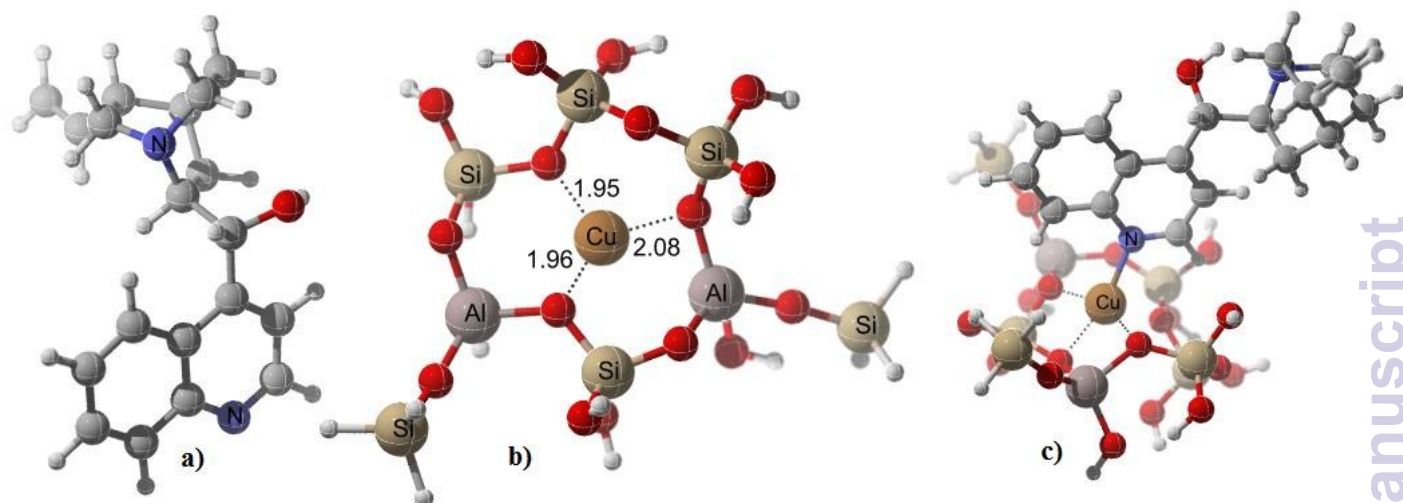


Figure 15. Optimized geometries of a) cinchonidine b) Cu²⁺-Y, c) Cu²⁺-Y-CD complex

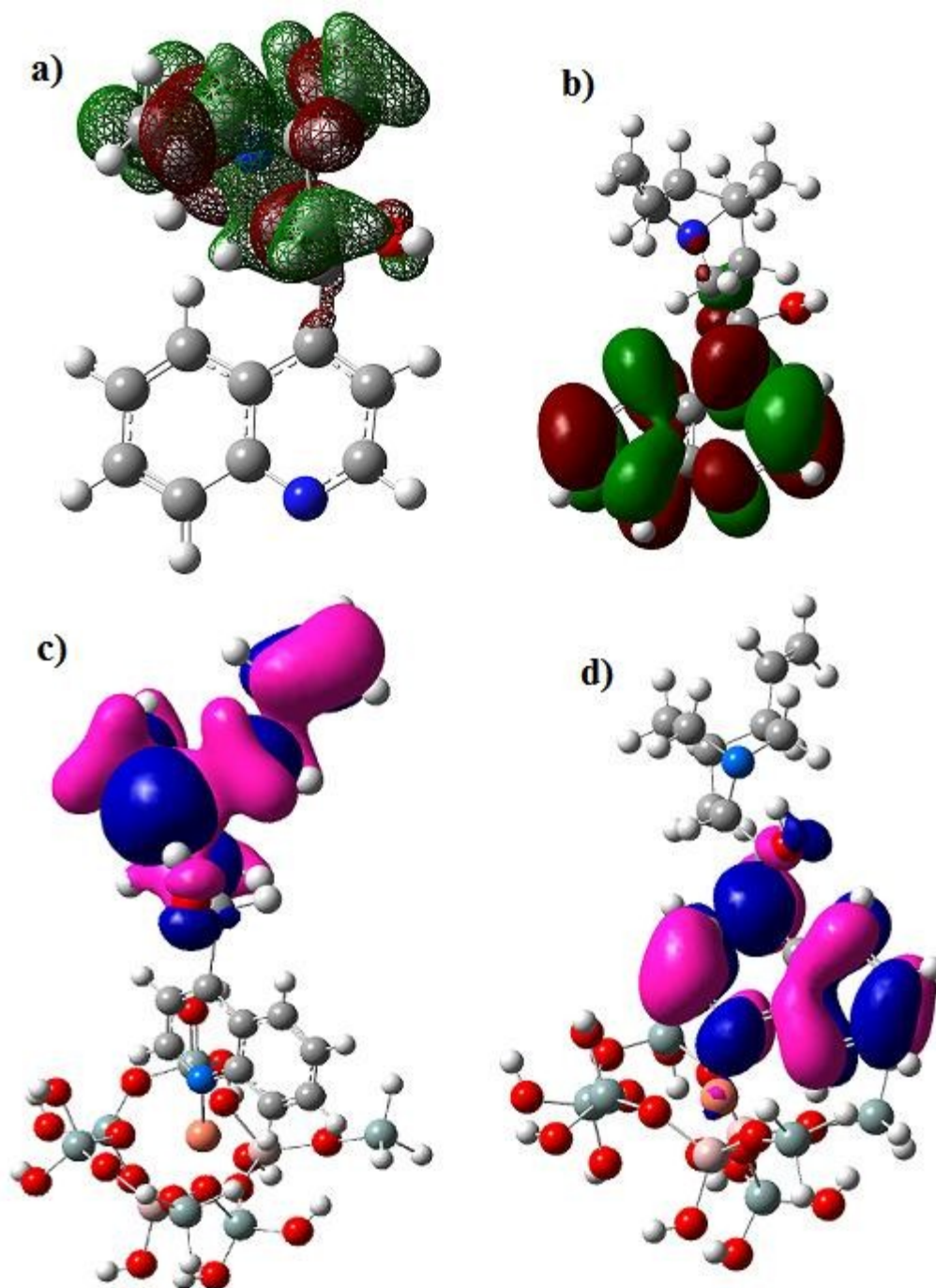
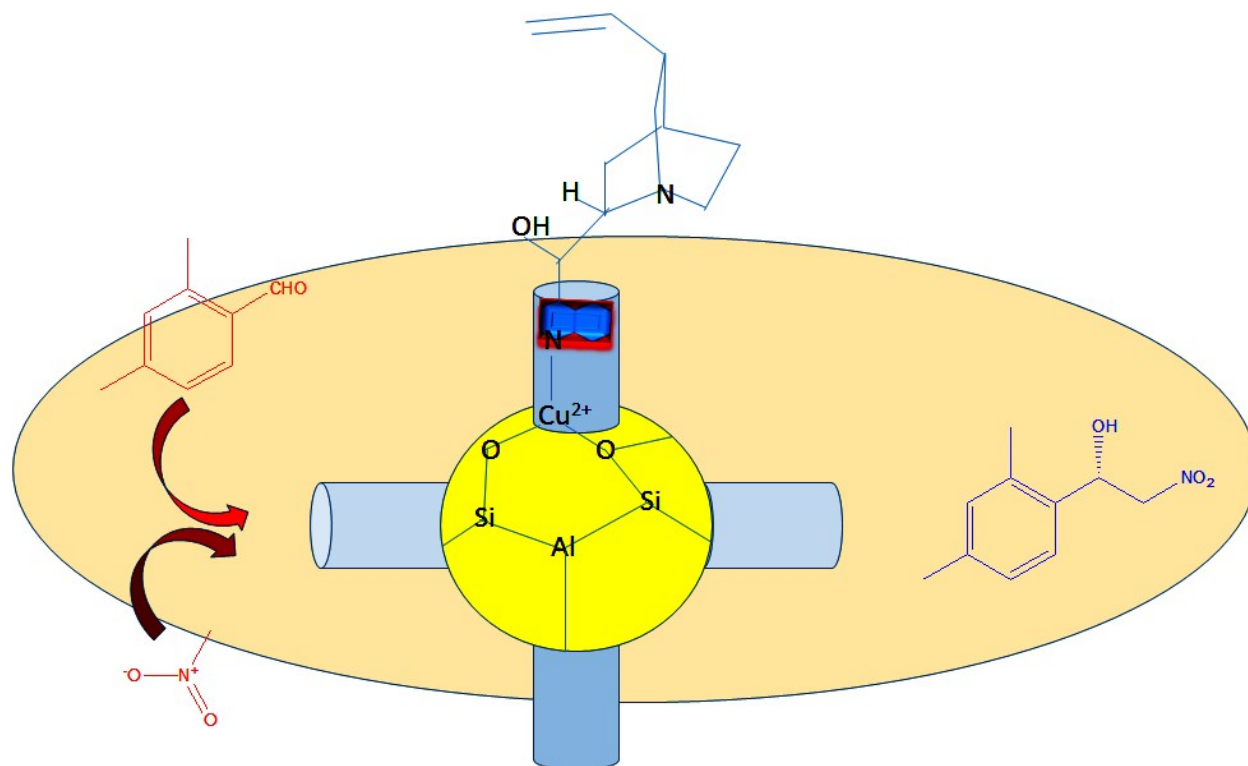


Figure 16. a) HOMO of cinchonidine, b) LUMO of cinchonidine, c) HOMO of Cu²⁺-Y-CD complex, d) LUMO of Cu²⁺-Y-CD complex

TOC

(-) cinchonidine is being encapsulated inside copper exchanged zeolite-Y and used as heterogeneous catalyst for asymmetric Henry reaction.